Geomechanics and Engineering, *Vol. 41, No. 5 (2025) 507-525*
https://doi.org/10.12989/gae.2025.41.5.507

Elastic instability analysis of functionally graded nanoplates under nonlinear coupling loads on a shear elastic foundation via non-local theory

Hayat Benachi[1,2a], Abderrahmane Menasria[1,3b], Abdelhakim Bouhadra[*1,3], Mourad Chitour[4c], Mohamed Ali Rachedi[1,3d], Belgacem Mamen[1,3e] and Abdelouahed Tounsi[**3,5]

[1]*Department of Civil Engineering, Faculty of Science and Technology, Abbès Laghrour University, Khenchela, Algeria*
[2]*Laboratoire d'Ingénierie et Sciences des Matériaux Avancés, Abbès Laghrour University, Khenchela, Algeria*
[3]*Material and Hydrology Laboratory, University of Sidi Bel Abbes, Faculty of Technology, Civil Engineering Department, Algeria*
[4]*Department of Mechanic Engineering, Faculty of Science and Technology, Abbès Laghrour University, Khenchela, Algeria*
[5]*Department of Civil and Environmental Engineering, King Fahd University of Petroleum & Minerals, 31261 Dhahran, Eastern Province, Saudi Arabia*

(*Received February 13, 2025, Revised April 26, 2025, Accepted May 14, 2025*)

Abstract. Nanostructures are generally used in environments where they can be subjected to different types of loading; understanding and determining their reaction to a hygro-thermo-mechanical environment is crucial for their design. This analysis's main objective is to evaluate the buckling sensitivity of sandwich nanoplates of FGMs subjected to a hygro-thermomechanical loading while resting on a two-parameter elastic medium. To accomplish this investigation, a quasi-3D high-shear deformation theory involving five variables containing integral terms, including the nonlocal elasticity theory of Eringen, is used. The assumed sandwich nanoplate is placed on an elastic medium, submitted to multiple boundary conditions, and subjected to a hygro-thermo-mechanical stress. The sandwich nameplate's material properties are intended to be continuously graded across its whole thickness. An elastic foundation with two parameters is used to model the elastic environment. The equilibrium equations are constructed using the concept of virtual displacements, and the solution is displayed for several boundary conditions. The obtained outcomes are approved and validated by comparison with those found by other scholars discussing the same topic in the literature. The impact and influence of various parameters on the stability of FGM sandwich nanoplates in a hygro-thermomechanical situation are investigated through the intermediary of parametric analysis.

Keywords: buckling; elastic foundation; Eringen; hygro-thermo-mechanical; nanoplates; nanostructures

1. Introduction

Functionally Graded Materials (FGMs) are advanced composite materials with continuously varying compositions and properties over a certain distance. These varying characteristics make these materials highly applicable for thermal barriers, aerospace components, and biomedical implants Hadj Mostefa *et al.* (2024). This analysis of FGM plates is based on various plate theories applicable to different situations. The Classical Plate Theory (CPT) targets thin plates using Kirchhoff-Love assumptions (Reissner and Stavsky (1961). However, this theory neglects shear deformation, which leads to potential inaccuracies for thick plates. The First-Order Shear Deformation Theory (FSDT) or Mindlin-Reissner theory is used for moderately thick plates, which accounts for shear deformation and utilises shear correction factors (Della Croce and Venini 2004, Trabelsi *et al.* 2018). To achieve better accuracy for a wide range of thicknesses, Higher-Order Shear Deformation Theories (HSDT) are employed to eliminate the introduction of shear correction factors. This was achieved by incorporating higher-order terms in the displacement field (Berkia *et al.* 2022, Himeur *et al.* 2022, Slimani *et al.* 2024, Tamrabet *et al.* 2024). When FGMs quickly change properties or are layered, the layer-wise theory (LT) divides the plate into many layers for effective analysis (Beg and Yasin 2021, Hadji *et al.* 2024, Komarsofla *et al.* 2021, Wei *et al.* 2024). However, this theory is complex and takes lots of time consuming. Nonlocal Plate Theories deal with size-dependent effects such as nonlocal elasticity at the nanoscale level.

The incorporation (use) of functional gradient materials (FGMs) in the design of various structural elements has become inevitable in the field of nanotechnology owing to the properties and advantageous effects of these innovative materials, which can overcome the problems or disadvantages associated with the use of conventional composite materials. Nanoplates manufactured from functional gradient materials are typically subjected to combined stresses in the environments in which they are designed. In addition to the fact that nanostructures can be

∗Corresponding author, Professor
E-mail: bouhadrahako@gmail.com
**Corresponding author, Professor
E-mail: tou_abdel@yahoo.com
[a]Ph.D. Student
[b]Ph.D.
[c]Ph.D.
[d]Ph.D.
[e]Ph.D.

ISSN: 2005-307X (Print), 2092-6219 (Online)

designed based on elastic foundations, their edges may have various boundary conditions. Researchers and experts specialising in these subjects have investigated and analysed these diverse criteria.

Among the recurring problems impacting nanoplates developed using FGMs is their buckling behaviour independent of their origin (mechanical, thermal, or both); this subject is very important in the research in progress. Consequently, multiple scholars have conducted extensive studies to assess the response of nanoplates that are susceptible to this phenomenon. Narendar (2011) initiated a study on the buckling of nano-isotropic plates by utilising a refined theory with two variables that considered nonlocal small effects. Nami *et al.* (2015) investigated the effect of thermal buckling on the response of rectangular FGM nanoplates using third-order theory. The same work was conducted by Farajpour *et al.* (2016), but this time for orthotropic nanoplates. In addition, Khorshidi and Fallah (2016) treated the case of nanoplate buckling using exponential shear deformation theory. In addition, to examine the size-dependent stability reaction of nanoplates with FGM's temperature-dependent material properties of FGMs, Karami and Karami (2019) developed a four-unknown improved plate theory using the Galerkin technique. Tong *et al.* (2021) included the size and surface effects in a third-order shear plate theory to study the elastic stability of nanoplates. Saberi *et al.* (2024) investigated the impact of a new model of porosity repartition on FGM nanoplates in the case of mechanical and thermal buckling.

Lazreg *et al*. (2023) investigate the elastic bending behavior of rectangular sandwich plates using a high-order theory that is variationally consistent and closely aligned with the classical plate theory in many respects. This approach eliminates the need for a shear correction factor and naturally accounts for the parabolic variation of transverse shear stresses across the thickness, satisfying the free surface conditions. The plate's material properties are assumed to vary through the thickness according to a simple power-law distribution based on the volume fractions of the constituent materials. Moreover, the proposed theory reduces the number of unknowns and equilibrium equations, thereby simplifying its application. Sedighi *et al.* (2020) investigated hybrid nanotubes, integrating carbon and boron-nitride nanotubes, as novel building blocks that combine the unique strengths of both materials concurrently. Additionally, blending these nanotubes with other materials enables the production of large-scale nanotubes, making them viable for macroscale applications. Abouelregal *et al.* (2021) explored the thermal and mechanical vibration characteristics of functionally graded microbeams. The governing equations were derived using the classical Euler–Bernoulli beam model integrated with the generalised dual-phase lag thermoelasticity model instead of the traditional steady-state Fourier heat conduction approach. The analysis assumes that the mechanical and thermal properties, including the modulus of elasticity, density, and thermal conductivity, vary exponentially with thickness, while Poisson's ratio remains constant.

In addition to mechanical loading, nanoplates can be subjected to other types of stress, such as thermal load and humidity effects. Understanding the impact of these various types of loading, individually or combined, on the behaviour of nanoplates composed of FGMs is essential to predict their reaction. Sari *et al.* (2020) analysed the behaviour of FGM nanoplates subjected simultaneously to thermal and mechanical loading. A supplementary investigation was conducted by Esen and Özmen (2024) on nanoplates that experienced free and forced vibration and buckling under combined mechanical and thermal loading. Recently, a hygro thermo elastic study was performed by Dhore *et al.* (2025), combining both temperature and moisture effects for the case of circular nanoplate while considering the memory effect.

Aside from the various loads that require nanoplates, different types of boundary and support conditions need to be considered to deepen our understanding of their consequences on the performance of these elements. Therefore, scientists and researchers have concentrated on this issue, seeking explanations and drawing conclusions about the effects of these parameters. The impact of varying the boundary conditions on the buckling of anisotropic nanoplates using Galerkin's approach was investigated by Karami *et al.* (2019). In another context, Bouhadra *et al.* (2021) analysed the stability of nanobeams subject to different boundary conditions. Uzun *et al.* (2023) also investigated the behaviour of nanobeams considering various boundary conditions, but this time by adding an elastic foundation and performing a vibration analysis. Recently, Daikh *et al.* (2023) used a quasi-3D theory to investigate the flexural reaction of nanoplates implanted in elastic foundations with four parameters, considering several boundary conditions. Moreover, the responses of nanoplates designed with a new range of FGMs (GPL-reinforced FGM) to bending and buckling were discussed by Nguyen *et al.* (2024). Furthermore, a similar study was conducted by Van Minh *et al.* (2024) to determine the reaction of flexo-magnetic nanoplates embedded in an elastic medium to buckling, free vibration, and static bending by considering geometrical imperfections. Cui *et al.* (2024) analysed the dynamic response of nanoparticle-reinforced porous beams using the Mori-Tanaka method to capture nanoparticle and pore interactions. Najafi *et al.* (2024) developed a 3D displacement-based model for the free vibration of functionally graded nanoplates on elastic foundations, employing nonlocal elasticity and power-law gradation. Liu *et al.* (2024) studied nonlinear vibrations in composite cylindrical shells with FG porous cores and CNT-reinforced layers, accounting for neutral surface effects. Shen *et al.* (2024) examined the free vibration of FG porous spherical caps with graphene platelet reinforcement and various porosity patterns. Eltaher *et al.* (2024) explored the dynamic, size-dependent responses of FGCNT nanoplates using the nonlocal strain gradient theory and multiple CNT configurations. Fan and She (2025) investigated the transient behaviour in graphene platelet-reinforced metal foam beams with initial geometric defects, considering different platelet and porosity distributions through advanced dynamic modelling.

Vibration analysis of nanostructures, including porous nanostructures and those resting on various types of elastic foundations. Tran and Le (2023) introduced a novel eight-node rectangular finite element (Q8) to formulate the motion equations of functionally graded porous nanoplates on elastic foundations based on the finite element method and nonlocal elasticity theory. Kumar *et al*. (2024)

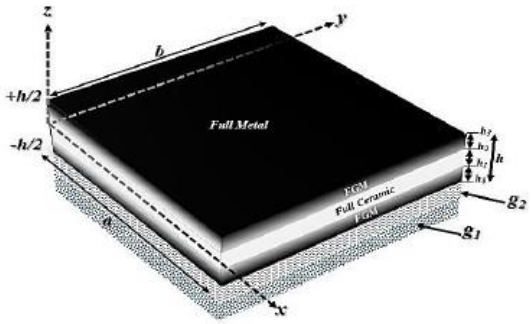

Fig. 1 The geometry of the FGM plate

investigated the dynamic response of imperfect functionally graded nanoplates resting on an elastic foundation, employing the Rayleigh–Ritz method to solve the governing equations of motion. Rai and Gupta (2024) were the first to develop a vibration stiffness matrix for analysing the dynamic behaviour of functionally graded nanoplates on a two-parameter elastic foundation, using nonlocal elasticity theory and Hamilton's principle to derive the governing equations. Son *et al.* (2025) studied the influence of thermal and nonlocal effects on the dynamic response of FG sandwich nanoplates supported by Winkler–Pasternak elastic foundations, employing nonlocal elasticity theory and Navier's solution to ensure frequency convergence across all mode sequences. Finally, Baghdali *et al.* (2025) examined both the equilibrium and dynamic behaviours of functionally graded nanostructures resting on viscoelastic supports with nonlocal equations derived using Hamilton's principle based on Eringen's elasticity theory.

This study investigates the buckling behaviour of functionally graded material (FGM) sandwich nanoplates supported by a two-parameter elastic foundation and subjected to hygro-thermo-mechanical loading under diverse boundary conditions. The novelty lies in the application of a simplified quasi-3D higher-order shear deformation theory with only five variables, integrated with Eringen's nonlocal elasticity theory through integral terms, to accurately capture nanoscale effects. The sandwich nanoplate, with continuously graded material properties across its thickness, experiences combined hygrothermal and mechanical stresses while resting on an elastic medium. Equilibrium equations were derived using the principle of virtual displacements, and solutions were provided for various boundary conditions. The accuracy of this formulation was validated by comparing the results with existing studies on similar problems. Additionally, a parametric analysis elucidated the effects of key factors on the stability of FGM nanoplates in hygro-thermo-mechanical environments.

2. Formulation

In this study, we used an FG sandwich nanoplate with length (a), width (b), and height (h) composed of three layers. The top and bottom layers consist of ceramic and metal (FGM), whereas the middle layer is made purely of ceramic. It was further assumed that an elastic foundation supported the FG sandwich nanoplates.

The material properties for each layer (j), such as the modulus of elasticity, Poisson's ratio (ν), coefficient of thermal expansion (α), and thermal expansion coefficient (β), are assumed to vary continuously in the thickness of the FG sandwich nanoplate and are defined by Radwan (2019)

$$P^{i}(z) = P_m + (P_c - P_m)V_c^{(n)} \tag{1}$$

The volume fraction $V^{n}(z)$ for each layer of ceramic is defined according to the power law as follows Bourada *et al.* (2012) and Tounsi *et al.* (2013)

$$\begin{cases} If\ z \in [h_0 ... h_1] \text{ then } \quad V^{1}(z) = \left(\dfrac{z-h_0}{h_1-h_0}\right)^{k} \\ If\ z \in [h_1 ... h_2] \text{ then } \quad V^{2}(z) = 1 \\ If\ z \in [h_2 ... h_3] \text{ then } \quad V^{3}(z) = \left(\dfrac{z-h_3}{h_2-h_3}\right)^{k} \end{cases} \tag{2}$$

where (k) is the material parameter, with (m) representing metal and (c) representing ceramic. The layer is considered entirely ceramic when the value of (k) is zero, and entirely metallic when (k) approaches infinity.

We have the FG sandwich nanoplate resting on two-parameter elastic foundations, defined by

$$R_f = g_1 w - g_2 \nabla^2 w \tag{3}$$

Where (R_f) is the force per unit area, (g_1) and (g_2) are the Winkler foundation stiffness and the shearing layer (Pasternak) stiffness.

2.1 Constitutive equations:

According to the nonlocal elasticity theory developed by Eringen (1983) and Eringen and Edelen (1972), the nonlocal constitutive relations of an FG sandwich nanoplate can be written as

$$\Im \begin{Bmatrix} \sigma_{xx} \\ \sigma_{yy} \\ \sigma_{zz} \\ \tau_{xz} \\ \tau_{yz} \\ \tau_{xy} \end{Bmatrix}^{(n)} = \begin{bmatrix} C_{11} & C_{12} & C_{13} & 0 & 0 & 0 \\ C_{12} & C_{22} & C_{23} & 0 & 0 & 0 \\ C_{13} & C_{23} & C_{33} & 0 & 0 & 0 \\ 0 & 0 & 0 & C_{44} & 0 & 0 \\ 0 & 0 & 0 & 0 & C_{55} & 0 \\ 0 & 0 & 0 & 0 & 0 & C_{66} \end{bmatrix}^{(n)} \begin{Bmatrix} \varepsilon_{xx}-\alpha T-\beta C \\ \varepsilon_{yy}-\alpha T-\beta C \\ \varepsilon_{zz}-\alpha T-\beta C \\ \gamma_{xz} \\ \gamma_{yz} \\ \gamma_{xy} \end{Bmatrix}^{(n)} \tag{4}$$

Where $(\sigma_x, \sigma_y, \sigma_z, \tau_{xy}, \tau_{yz}, \tau_{xz})$ and $(\varepsilon_x, \varepsilon_y, \varepsilon_z, \gamma_{xy}, \gamma_{yz}, \gamma_{xz})$ are The components of stresses and strains, respectively.

The stiffness coefficients $C_{ij}^{(n)}$ for each layer can be written as follows

$$\begin{aligned} C_{11}^{(n)} = C_{22}^{(n)} = C_{33}^{(n)} &= \frac{E^{(n)}(z)(1-\nu)}{(1-2\nu)(1+\nu)} \\ C_{12}^{(n)} = C_{13}^{(n)} = C_{23}^{(n)} &= \frac{\nu E^{(n)}(z)}{(1-2\nu)(1+\nu)} \\ C_{44}^{(n)} = C_{55}^{(n)} = C_{66}^{(n)} &= \frac{E^{(n)}(z)}{2(1+\nu)} \end{aligned} \tag{5}$$

The nonlocal operator $\Im$ is defined as

$$\Im = 1 - \mu^2 \nabla^2 \tag{6}$$

Where $\mu = e_0\ell$ represents a nonlocal coefficient that reveals the effects of small scales in nanostructures. In this case, ℓ denotes an internal characteristic length while e_0 does Eringen's present a constant Eringen (1983) as follows

$$e_0 = \frac{\sqrt{\pi^2 - 4}}{2\pi} \tag{7}$$

2.2 Kinematics and strains

The displacement field of high-order shear deformation theory (HSDT) is expressed as follows

$$\begin{aligned} u(x,y,z) &= u_0 - z\frac{dw_0}{dx} + f(z)K_1\int\theta dx \\ u(x,y,z) &= u_0 - z\frac{dw_0}{dy} + f(z)K_2\int\theta dy \\ w(x,y,z) &= w_0 + g(z)\varphi(z) \end{aligned} \tag{8}$$

u_0, v_0 and w_0 are the mid-plane displacements, the coefficients k_1 and k_2 depend on the geometry.

The following formula provides a modified shape function

$$f(z) = \left(\frac{z}{\pi}\right)\left(\frac{1}{\pi^{3\pi}} + \left(\frac{h}{z}\right)\sin\left(\frac{\pi z}{h}\right)\right)$$

and (9)

$$g(z) = \frac{\partial f(z)}{\partial z}$$

The strain components ε_{ij} are obtained from the above displacement field (5) as follows:

$$\begin{aligned} \varepsilon_{xx} &= \varepsilon^0_{xx} + z\varepsilon^1_{xx} + f(z)\varepsilon^2_{xx} \\ \varepsilon_{yy} &= \varepsilon^0_{yy} + z\varepsilon^1_{yy} + f(z)\varepsilon^2_{yy} \\ \varepsilon_{zz} &= \frac{\partial g(z)}{\partial z}\varepsilon^0_{zz} \\ \gamma_{xy} &= \gamma^0_{xy} + z\gamma^1_{xy} + f(z)\gamma^2_{xy} \\ \gamma_{yz} &= \frac{\partial f(z)}{\partial z}\left(\gamma^0_{yz} + \gamma^1_{yz}\right) \\ \gamma_{xz} &= \frac{\partial f(z)}{\partial z}\left(\gamma^0_{xz} + \gamma^1_{xz}\right) \end{aligned} \tag{10}$$

Where

$$\begin{Bmatrix} \varepsilon^0_{xx} \\ \varepsilon^0_{yy} \\ \gamma^0_{xy} \end{Bmatrix} = \begin{Bmatrix} \partial u_0/\partial x \\ \partial v_0/\partial y \\ \partial u_0/\partial y + \partial v_0/\partial x \end{Bmatrix}, \begin{Bmatrix} \varepsilon^1_{xx} \\ \varepsilon^1_{yy} \\ \varepsilon^1_{xy} \end{Bmatrix} = \begin{Bmatrix} -\partial^2 w_0/\partial x^2 \\ -\partial^2 w_0/\partial y^2 \\ -2\partial^2 w_0/\partial x\partial y w \end{Bmatrix} \tag{11a}$$

$$\begin{Bmatrix} \varepsilon^2_{xx} \\ \varepsilon^2_{yy} \\ \varepsilon^2_{xy} \end{Bmatrix} = \begin{Bmatrix} K_1 A\left(\dfrac{\partial^2\theta}{\partial x^2}\right) \\ K_2 B\left(\dfrac{\partial^2\theta}{\partial y^2}\right) \\ (K_1 A + K_2 B)\left(\dfrac{\partial^2\theta}{\partial x\partial y}\right) \end{Bmatrix}$$

$$\begin{Bmatrix} \gamma^0_{xz} \\ \gamma^0_{yz} \end{Bmatrix} = \begin{Bmatrix} K_1 A\left(\dfrac{\partial\theta}{\partial x}\right) \\ K_2 B\left(\dfrac{\partial\theta}{\partial y}\right) \end{Bmatrix}, \begin{Bmatrix} \gamma^1_{xz} \\ \gamma^1_{yz} \end{Bmatrix} = \begin{Bmatrix} \dfrac{\partial\theta}{\partial x} \\ \dfrac{\partial\theta}{\partial y} \end{Bmatrix} \tag{11b}$$

The integrals specified in the above equations are evaluated using Navier's method and can be formulated as follows

$$\int\theta dx = A'\left(\frac{\partial\theta}{\partial x}\right) \quad \text{and} \quad \int\theta dy = B'\left(\frac{\partial\theta}{\partial y}\right) \tag{12a}$$

The coefficients A′, B′, k_1 and k_2 are determined based on the type of solution used, in this case, Navier's method. The coefficients A′, B′, k_1 and k_2 are given as follows

$$K_1 = \lambda^2, \quad K_2 = \eta^2, \quad A' = -\frac{1}{\lambda^2} \text{ and } B' = -\frac{1}{\eta^2} \tag{12b}$$

Where

$$\lambda = \frac{m\pi}{a} \text{ and } \eta = \frac{n\pi}{b} \tag{12c}$$

2.3 Stability equations

The principle of virtual displacements can be utilised to derive the equilibrium equation for the current problem

$$\int_V (\delta U + \delta V)dV = 0 \tag{13}$$

The variation in the strain energy can be expressed as

$$\delta U = \int_V \begin{bmatrix} \sigma_{xx}\,\delta\varepsilon_{xx} + \sigma_{yy}\,\delta\varepsilon_{yy} + \sigma_{zz}\,\delta\varepsilon_{zz} \\ +\tau_{xy}\,\delta\gamma xy + \tau_{yz}\,\delta\gamma_{yz} + \tau_{xz}\,\delta\gamma_{xz} \end{bmatrix} dV \tag{14a}$$

$$U = \int_\Omega \begin{bmatrix} N_{xx}\,\delta\varepsilon^0_{xx} + M_{xx}\,\delta\varepsilon^1_{xx} + P_{xx}\,\delta\varepsilon^2_{xx} \\ +N_{yy}\,\delta\varepsilon^0_{yy} + M_{yy}\,\delta\varepsilon^1_{yy} + P_{yy}\,\delta\varepsilon^2_{yy} \\ +N_{zz}\,\delta\varepsilon^0_{zz} + N_{xy}\,\delta\varepsilon^0_{xy} + M_{xy}\,\delta\varepsilon^1_{xy} \\ +P_{xy}\,\delta\varepsilon^2_{xy} + Q_{yz}\delta\gamma^0_{yz} + Q_{xz}\,\delta\gamma^0_{xz} \\ +S_{yz}\delta\gamma^1_{yz} + S_{xz}\,\delta\gamma^1_{xz} \end{bmatrix} dA \tag{14b}$$

Where N, M, and S are the resultant forces defined as follows

$$\begin{aligned} \left(N_i, M^b_i, M^s_i\right)^{(n)} &= \sum_{j=1}^{3}\int_{h_{j-1}}^{h_j}(1, z, f(z))\sigma^{(j)}_i dz \quad \text{with } (i = x, y, xy) \\ N_z{}^{(n)} &= \sum_{j=1}^{3}\int_{h_{j-1}}^{h_j} f''(z)\sigma^{(j)}_z dz \\ \left(S^s_{xz}, S^s_{yz}\right)^{(n)} &= \sum_{j=1}^{3}\int_{h_{j-1}}^{h_j} f'(z)\left(\tau_{xz}, \tau_{yz}\right)^{(j)} dz \end{aligned} \tag{15}$$

The variation in the external work can be expressed as

$$\begin{aligned} \delta V &= \int_A \left(-R_f\delta w + \left[F_x\frac{\partial w}{\partial x}\frac{\partial\delta w}{\partial x} + F_y\frac{\partial w}{\partial y}\frac{\partial\delta w}{\partial y}\right]\right)dA \\ &= \int_A \left(\begin{bmatrix} -R_f\delta\left(w_0 + f'(z)\varphi_z\right) \\ +\left[F_x\dfrac{\partial\left(w_0 + f'(z)\varphi_z\right)}{\partial x}\dfrac{\partial\delta\left(w_0 + f'(z)\varphi_z\right)}{\partial x}\right. \\ \left.+F_y\dfrac{\partial\left(w_0 + f'(z)\varphi_z\right)}{\partial y}\dfrac{\partial\delta\left(w_0 + f'(z)\varphi_z\right)}{\partial y}\right] \end{bmatrix}\right)dA \end{aligned} \tag{16}$$

After substituting Eqs. (14(b)) and (16) into equation (13) and by using the integration by parts, the equilibrium equations for the plate are obtained by isolating the

coefficients of u_0 , δv_0 , δw_0 , $\delta\theta$ and $\delta\varphi_z$.

$$
\begin{aligned}
&\delta u_0 : \frac{\partial N_{xx}}{\partial x}+\frac{\partial N_{xy}}{\partial y}=0\\
&\delta v_0 : \frac{\partial N_{xy}}{\partial x}+\frac{\partial N_{yy}}{\partial y}=0\\
&\delta w_0 : \frac{\partial^2 M_{xx}}{\partial x^2}+2\frac{\partial^2 M_{xy}}{\partial x\partial y}+\frac{\partial^2 M_{yy}}{\partial y^2}-R_f+F_x\frac{\partial^2}{\partial x^2}(w_0+f'(z)\varphi_z)\\
&\quad +F_y\frac{\partial^2}{\partial y^2}(w_0+f'(z)\varphi_z)=0\\
&\delta\theta : -K_1A\frac{\partial^2 P_{xx}}{\partial x^2}-K_2B\frac{\partial^2 P_{yy}}{\partial y^2}-(K_1A+K_2B)\frac{\partial^2 P_{xy}}{\partial x\partial y}+K_1A\frac{\partial S_{xz}}{\partial x}\\
&\quad + K_2B\frac{\partial S_{yz}}{\partial y}=0\\
&\delta\varphi : \frac{\partial Q_{xz}}{\partial x}+\frac{\partial Q_{yz}}{\partial y}-N_{zz}-f'(z)R_f+F_xf'(z)\frac{\partial^2}{\partial x^2}(w_0+f'(z)\varphi_z)\\
&\quad +F_yf'(z)\frac{\partial^2}{\partial y^2}(w_0+f'(z)\varphi_z)=0
\end{aligned}
\tag{17}
$$

The stability equations of the nanoplate can be derived based on the neighbouring equilibrium criterion. It is assumed that the equilibrium state of the functionally graded material (FGM) nanoplate, under hygrothermal loading, is defined by its displacement components. u_0^0 , v_0^0 , w_0^0 , θ_0^0 *and* φ_0^0.

The components of a neighbouring stable state are different by u_0^1 , v_0^1 , w_0^1 , θ_0^1 *and* φ_0^1, from the equilibrium position. Therefore, the total displacements of the neighbouring states are expressed as in Meziane *et al.* (2014).

$$
\begin{aligned}
u_0 = u_0^0+u_0^1,\ v_0 = v_0^0+v_0^1\\
w_0 = w_0^0+w_0^1\\
\theta=\theta^0+\theta^1 \quad \text{and} \quad \phi_z=\varphi_z^0+\varphi_z^1
\end{aligned}
\tag{18}
$$

Similarly, the force resultants of a neighbouring state may be expressed concerning the equilibrium state as follows

$$
\begin{aligned}
N_i = N_i^0+N_i^1 \ \text{ with } \ i=x,y,xy \text{ and } z\\
M_i^b = M_i^{b0}+M_i^{b1},\ M_i^s = M_i^{s0}+M_i^{s1} \ \text{ with } \ i=x,y,xy\\
S_i^s = S_i^{s0}+S_i^{s1} \text{ with } \ i=xz,yz
\end{aligned}
\tag{19}
$$

The stability equations were derived by substituting Eqs. (18) and (19) into Eq. (17). After substitution, the terms with superscript 0 that satisfy the equilibrium condition are removed from the resulting equations.

$$
\begin{aligned}
&\delta u_0^1 : \frac{\partial N^1{}_{xx}}{\partial x}+\frac{\partial N^1{}_{xy}}{\partial y}=0\\
&\delta v_0^1 : \frac{\partial N^1{}_{xy}}{\partial x}+\frac{\partial N^1{}_{yy}}{\partial y}=0\\
&\delta w_0^1 : \frac{\partial^2 M^{b1}{}_{xx}}{\partial x^2}+2\frac{\partial^2 M^{b1}{}_{xy}}{\partial x\partial y}+\frac{\partial^2 M^{b1}{}_{yy}}{\partial y^2}-R_f\\
&\quad +F_x\frac{\partial^2}{\partial x^2}\left(w^1{}_0+f'(z)\varphi^1{}_z\right)+F_y\frac{\partial^2}{\partial y^2}\left(w^1{}_0+f'(z)\varphi^1{}_z\right)=0\\
&\delta\theta^1 : -K_1A\frac{\partial^2 M^{s1}{}_{xx}}{\partial x^2}-K_2B\frac{\partial^2 M^{s1}{}_{yy}}{\partial y^2}-(K_1A+K_2B)\frac{\partial^2 M^{s1}{}_{xy}}{\partial x\partial y}\\
&\quad +K_1A\frac{\partial S^{s1}{}_{xz}}{\partial x}+K_2B\frac{\partial S^{s1}{}_{yz}}{\partial y}=0\\
&\delta\varphi^1 : \frac{\partial S^{s1}{}_{xz}}{\partial x}+\frac{\partial S^{s1}{}_{yz}}{\partial y}-N^1{}_{zz}-f'(z)R_f\\
&\quad +F_xf'(z)\frac{\partial^2}{\partial x^2}\left(w^1{}_0+f'(z)\varphi^1{}_z\right)+F_yf'(z)\frac{\partial^2}{\partial y^2}\left(w^1{}_0+f'(z)\varphi^1{}_z\right)=0
\end{aligned}
\tag{20}
$$

The in-plane edge loads F_i are written as:

$$
F_x = p_x+N_x^T+N_x^C \ \text{ and } \ F_y = p_y+N_y^T+N_y^C \tag{21}
$$

Where (p_x, p_y) and $(N_x^T, N_y^T, N_x^C, N_y^C)$ represent the normal in-plane forces caused by mechanical and temperature loads, respectively.

$$
\begin{aligned}
&p_x = p_y = p\\
&N_x^T = N_y^T = N^T = -\sum_{j=1}^{3}\int_{h_{j-1}}^{h_j}\frac{E^{(j)}(z)}{1-\nu}\alpha^{(j)}(z)\Delta T dz\\
&N_x^C = N_y^C = N^C = -\sum_{j=1}^{3}\int_{h_{j-1}}^{h_j}\frac{E^{(j)}(z)}{1-\nu}\beta^{(j)}(z)\Delta T dz
\end{aligned}
\tag{22}
$$

By replacing equation (III.12) in equation (III.6) and substituting the resultant forces in equation (III.18), the resulting stresses are as follows

$$
\begin{Bmatrix} N^1{}_x\\ N^1{}_y\\ N^1{}_{xy}\\ M^{b1}_x\\ M^{b1}_y\\ M^{b1}_{xy}\\ M^{s1}_x\\ M^{s1}_y\\ M^{s1}_{xy}\\ N^1{}_z \end{Bmatrix} = \begin{bmatrix} A_{11} & A_{12} & 0 & B_{11} & B_{12} & 0 & B^s_{11} & B^s_{12} & 0 & X_{13}\\ A_{12} & A_{22} & 0 & B_{12} & B_{22} & 0 & B^s_{12} & B^s_{22} & 0 & X_{23}\\ 0 & 0 & A_{66} & 0 & 0 & B_{66} & 0 & 0 & B^s_{66} & 0\\ B_{11} & B_{12} & 0 & D_{11} & D_{12} & 0 & D^s_{11} & D^s_{12} & 0 & Y_{13}\\ B_{12} & B_{22} & 0 & D_{12} & D_{22} & 0 & D^s_{12} & D^s_{22} & 0 & Y_{23}\\ 0 & 0 & B_{66} & 0 & 0 & D_{66} & 0 & 0 & D^s_{66} & 0\\ B^s_{11} & B^s_{12} & 0 & D^s_{11} & D^s_{12} & 0 & H^s_{11} & H^s_{12} & 0 & Y^s_{13}\\ B^s_{12} & B^s_{22} & 0 & D^s_{12} & D^s_{22} & 0 & H^s_{12} & H^s_{22} & 0 & Y^s_{23}\\ 0 & 0 & B^s_{66} & 0 & 0 & D^s_{66} & 0 & 0 & H^s_{66} & 0\\ X_{13} & X_{23} & 0 & Y_{13} & Y_{23} & 0 & Y^s_{13} & Y^s_{23} & 0 & Z_{33} \end{bmatrix} \begin{Bmatrix} \varepsilon^0_x\\ \varepsilon^0_y\\ \gamma^0_{xy}\\ K^b_x\\ K^b_y\\ K^b_{xy}\\ K^s_x\\ K^s_y\\ K^s_{xy}\\ \varepsilon^0_z \end{Bmatrix} - \begin{Bmatrix} N^T_x\\ N^T_x\\ 0\\ M^{bT}_x\\ M^{bT}_x\\ 0\\ M^{sT}_x\\ M^{sT}_x\\ 0\\ N^T_z \end{Bmatrix} - \begin{Bmatrix} N^C_x\\ N^C_x\\ 0\\ M^{bC}_x\\ M^{bC}_x\\ 0\\ M^{sC}_x\\ M^{sC}_x\\ 0\\ N^C_z \end{Bmatrix} \tag{23a}
$$

$$
\begin{Bmatrix} S^s_{yz}\\ S^s_{xz} \end{Bmatrix} = \begin{bmatrix} A^s_{44} & 0\\ 0 & A^s_{55} \end{bmatrix} \begin{Bmatrix} \gamma^0_{yz}\\ \gamma^0_{xz} \end{Bmatrix} \tag{23b}
$$

The forces in the (z) direction are ignored because buckling primarily depends on the stresses in the (x) and (y) directions. This simplification makes the calculations easier without significantly affecting the accuracy of the buckling results.

Where

$$
\begin{aligned}
&\begin{Bmatrix} A_{11} & B_{11} & D_{11} & B^s_{11} & D^s_{11} & H^s_{11}\\ A_{12} & B_{12} & D_{12} & B^s_{12} & D^s_{12} & H^s_{12}\\ A_{66} & B_{66} & D_{66} & B^s_{66} & D^s_{66} & H^s_{66} \end{Bmatrix} =\\
&\int_{-h/2}^{h/2}\left[1,\ z,\ z^2,\ f(z),\ z\,f(z),\ f^2(z)\right] \begin{Bmatrix} C^{(n)}{}_{11}(z)\\ C^{(n)}{}_{12}(z)\\ C^{(n)}{}_{66}(z) \end{Bmatrix} dz
\end{aligned}
\tag{24}
$$

$$
\begin{Bmatrix} A^s_{44} & 0\\ 0 & A^s_{55} \end{Bmatrix} = \int_{-h/2}^{h/2}\left[f'(z)\right]^2 \begin{Bmatrix} C^{(n)}{}_{44}(z)\\ C^{(n)}{}_{55}(z) \end{Bmatrix} dz \tag{25}
$$

$$
\begin{aligned}
&\begin{Bmatrix} X_{ij} & Y_{ij} & Y^s_{ij} & Z_{ij} \end{Bmatrix} =\\
&\sum_{j=1}^{3} C^{(n)}{}_{ij}(z)\left[1, z, f(z), f'(z)\right] f'(z) dz \text{ and } (i=\ 4,\ 5)
\end{aligned}
\tag{26}
$$

The stress and moment results $N_x^\Theta = N_y^\Theta$; $M_x^{b\Theta} = M_y^{b\Theta}$ and $M_x^{s\Theta} = M_y^{s\Theta}$; (Θ=T, C) resulting from hygrothermal loading are given by

$$
\begin{Bmatrix} N_x^\Theta\\ M_x^{b\Theta}\\ M_x^{s\Theta} \end{Bmatrix} = \sum_{j=1}^{3}\frac{E^{(n)}(z)}{1-\nu^2}\Upsilon^{(n)}\Theta(z) \begin{Bmatrix} 1\\ z\\ f(z) \end{Bmatrix} dz \tag{27}
$$

$$\Theta(z)=\begin{cases}T(z) \;\; if \;\; \Upsilon=\alpha\\ C(z) \;\; if \;\; \Upsilon=\beta\end{cases} \tag{28}$$

By inserting equation (III.23) into equation (III.22), the governing equations of stability can be formulated in terms of the displacements (u_0 , v_0 , w_0 , θ , φ_z)

$$\begin{aligned}\delta u^1_0 :\; & A_{11}\frac{\partial^2 u^1_0}{\partial x^2}+A_{66}\frac{\partial^2 u^1_0}{\partial y^2}+(A_{12}+A_{66})\frac{\partial^2 v^1_0}{\partial x\partial y}\\ & +B_{11}\frac{\partial^3 w^1_0}{\partial x^3}-(B_{12}+2B_{66})\frac{\partial^3 w^1_0}{\partial x\partial y^2}+Bs_{11}K_1A\frac{\partial^3\theta^1}{\partial x^3}\\ & +(Bs_{12}K_2B+Bs_{66}(K_1A+K_2B))\frac{\partial^3\theta^1}{\partial x\partial y^2}+X_{13}\frac{\partial\varphi^1_z}{\partial x}=0\end{aligned} \tag{29a}$$

$$\begin{aligned}\delta v^1_0 :\; & (A_{12}+A_{66})\frac{\partial^2 u^1_0}{\partial x\partial y}+A_{22}\frac{\partial^2 v^1_0}{\partial y^2}+A_{66}\frac{\partial^2 v^1_0}{\partial x^2}\\ & -B_{22}\frac{\partial^3 w^1_0}{\partial y^3}-(B_{12}+2B_{66})\frac{\partial^3 w^1_0}{\partial x^2\partial y}+Bs_{22}K_2B\frac{\partial^3\theta^1}{\partial y^3}\\ & +(Bs_{12}K_1A+Bs_{66}(K_1A+K_2B))\frac{\partial^3\theta^1}{\partial x^2\partial y}+X_{23}\frac{\partial\varphi^1_z}{\partial y}=0\end{aligned} \tag{29b}$$

$$\begin{aligned}\delta w^1_0 :\; & B_{11}\frac{\partial^3 u^1_0}{\partial x^3}+(B_{12}+2B_{66})\frac{\partial^3 u^1_0}{\partial x\partial y^2}+B_{22}\frac{\partial^3 v^1_0}{\partial y^3}\\ & +(B_{12}+2B_{66})\frac{\partial^3 v^1_0}{\partial x^2\partial y}-D_{11}\frac{\partial^4 w^1_0}{\partial x^4}-D_{22}\frac{\partial^4 w^1_0}{\partial y^4}\\ & -2(D_{12}+2D_{66})\frac{\partial^4 w^1_0}{\partial x^2\partial y^2}+Ds_{11}K_1A\frac{\partial^4\theta^1}{\partial x^4}+Ds_{22}K_2B\frac{\partial^4\theta^1}{\partial y^4}\\ & +(Ds_{12}+2Ds_{66})(K_1A+K_2B)\frac{\partial^4\theta^1}{\partial x^2\partial y^2}+Y_{13}\frac{\partial^2\varphi^1}{\partial x^2}+Y_{23}\frac{\partial^2\varphi^1}{\partial y^2}\\ & +N^0_x\frac{\partial^2 w^1_0}{\partial x^2}+N^0_{xy}\frac{\partial^2 w^1_0}{\partial x\partial y}+N^0_y\frac{\partial^2 w^1_0}{\partial y^2}\\ & +\left(1-\mu^2\nabla^2\right)\left(\left(-p+N^T+N^C\right)\nabla^2(w^1_0+f'(z)\varphi^1_z)-R_f\right)=0\end{aligned} \tag{29c}$$

$$\begin{aligned}\delta\theta^1 :\; & -Bs_{11}K_1A\frac{\partial^3 u^1_0}{\partial x^3}-(Bs_{12}K_2B+Bs_{66}(K_1A+K_2B))\frac{\partial^3 u^1_0}{\partial x\partial y^2}\\ & -Bs_{22}K_2B\frac{\partial^3 v^1_0}{\partial x^3}-(Bs_{12}K_1A+Bs_{66}(K_1A+K_2B))\frac{\partial^3 v^1_0}{\partial x^2\partial y}\\ & +Ds_{11}K_1A\frac{\partial^4 w^1_0}{\partial x^4}+Ds_{22}K_2B\frac{\partial^4 w^1_0}{\partial y^4}+(K_1A+K_2B)(Ds_{12}+2Dss_{66})\frac{\partial^4 w^1_0}{\partial x^2\partial y^2}\\ & -Hs_{11}(K_1A)^2\frac{\partial^4\theta^1}{\partial x^4}-Hs_{22}(K_2B)^2\frac{\partial^4\theta^1}{\partial y^4}-2Hs_{12}(K_1A)(K_2B)\\ & +Hs_{66}(K_1A+K_2B)^2)\frac{\partial^4\theta^1}{\partial x^2\partial x^2}+(K_1A)^2As_{44}\frac{\partial^2\theta^1}{\partial x^2}+(K_2A)^2As_{55}\frac{\partial^2\theta^1}{\partial y^2}\\ & +Y^s_{13}K_1A\frac{\partial^2\varphi^1_z}{\partial x^2}+Y^s_{23}K_2B\frac{\partial^2\varphi^1_z}{\partial y^2}+(K_1A)As_{44}\frac{\partial^2\varphi^1_z}{\partial x^2}+(K_2B)As_{55}\frac{\partial^2\varphi^1_z}{\partial y^2}=0\end{aligned} \tag{29d}$$

$$\begin{aligned}\partial\varphi^1 :\; & X_{13}\frac{\partial u^1_0}{\partial x}+X_{23}\frac{\partial v^1_0}{\partial y}+Y_{13}\frac{\partial^2 w^1_0}{\partial x^2}+Y_{23}\frac{\partial^2 w^1_0}{\partial y}\\ & -(Ys_{13}+As_{44})K_1A\frac{\partial^2\theta^1}{\partial x^2}-(Ys_{23}+As_{55})K_2B\frac{\partial^2\theta^1}{\partial y^2}\\ & +As_{44}K_2B\frac{\partial^2\varphi^1_z}{\partial x^2}+As_{55}\frac{\partial^2\varphi^1_z}{\partial y^2}-Z_{33}\varphi^1_z\\ & +\left(1-\mu^2\nabla^2\right)\left[\begin{pmatrix}\left(-p+N^T+N^C\right)\nabla^2 f'(z)(w^1_0\\ +f'(z)\varphi^1_z)\end{pmatrix}-f'(z)R_f\right]=0\end{aligned} \tag{29e}$$

2.4 Types of hygrothermal change

We focused on three hygrothermal load types: uniform, linear, or non-linear hygrothermal distributions through the plate thickness. Refrafi *et al.* (2020).

2.4.1 Uniform hygrothermal rise (UHR)

At the beginning, the plate is subjected to an initial temperature and moisture content of (T_i) and (C_i) .Afterward, the temperature and moisture levels are uniformly elevated to final values of (T_f) and (C_f).

The hygrothermal effect on the nanoplate is given as

$$\Theta(z)=\Theta_f-\Theta_i=\Delta\Theta \;\text{ with }\; \Theta=T,C \tag{30a}$$

2.4.2 Linear hygrothermal rise (LHR)

The hygrothermal states at the lower and upper surfaces of the plate are denoted as Θ_l and Θ_u respectively. Consequently, the linear hygrothermal change across the thickness is expressed as

$$\Theta(z)=\Delta\Theta\left(\frac{1}{2}+\frac{z}{h}\right)+\Theta_l \tag{30b}$$

2.4.3 Non-linear hygrothermal rise (NHR)

In the first case, the temperature and moisture concentration at the top surface is T_t, C_t, and it is assumed to vary from T_t, C_t to T_b, C_b , T_b at which the plate buckles, following a power law variation through the thickness. Therefore, the temperature and moisture concentration rise through the thickness can be expressed as

$$\Theta(z)=\Delta\Theta\left(\frac{1}{2}+\frac{z}{h}\right)^{\gamma}+\Theta_l \tag{30c}$$

With the hygrothermal exponent, $1<\gamma<\infty$

2.5 Analytical solution

A solution for Eq. (29) for the functionally graded sandwich nanoplate under various boundary conditions can be constructed. A general solution for the boundary conditions is utilised to solve the governing equations. For this purpose, the displacement field can be expressed as

$$\begin{Bmatrix}u_0(x,y)\\ v_0(x,y)\\ w_0(x,y)\\ \theta(x,y)\\ \varphi_z(x,y)\end{Bmatrix}=\begin{Bmatrix}U_{mn} & X'_m(x)\,Y_n(y)\\ V_{mn} & X_m(x)Y'_n(y)\\ W_{mn} & X_m(x)Y_n(y)\\ \theta_{mn} & X_m(x)Y_n(y)\\ \phi_{mn} & X_m(x)Y_n(y)\end{Bmatrix} \tag{31}$$

U_{mn}, V_{mn}, W_{mn}, X_{mn} and ϕ_{mn} are arbitrary parameters that need to be determined.

The functions $X_m(x)$ and $Y_n(y)$ are proposed to meet the geometric boundary conditions. These functions, are presented in Table 1.

Inserting Equation (31) into Equation (29), the resulting Equations can be written as follows

$$\begin{bmatrix}S_{11} & S_{12} & S_{13} & S_{14} & S_{15}\\ & S_{22} & S_{23} & S_{24} & S_{25}\\ & & S_{33}+S_1 & S_{34} & S_{35}+S_2\\ & SYM & & S_{44} & S_{45}\\ & & & & S_{55}+S_3\end{bmatrix}\begin{Bmatrix}U_{mn}\\ V_{mn}\\ W_{mn}\\ X_{mn}\\ \Phi_{mn}\end{Bmatrix}=\begin{Bmatrix}0\\0\\0\\0\\0\end{Bmatrix} \tag{32}$$

Table 1 Admissible functions Xm(x) and Yn(y) (Mekerbi *et al.* 2021, Meziane *et al.* 2014)

	Boundary conditions		Functions X_m and Y_n	
	at x= 0,a	at y= 0,b	$X_m(x)$	$Y_n(y)$
SSSS	$X_m(0)=X_m^{"}(0)=0$ $X_m(a)=X_m^{"}(a)=0$	$Y_n(0)=Y_n^{"}(0)=0$ $Y_n(b)=Y_n^{"}(b)=0$	$\sin(\lambda x)$	$\sin(\mu y)$
CSSS	$X_m(0)=X_m^{'}(0)=0$ $X_m(a)=X_m^{"}(a)=0$	$Y_n(0)=Y_n^{"}(0)=0$ $Y_n(b)=Y_n^{"}(b)=0$	$\sin(\lambda x)\left[\cos(\lambda x)-1\right]$	$\sin(\mu y)$
CSCS	$X_m(0)=X_m^{'}(0)=0$ $X_m(a)=X_m^{"}(a)=0$	$Y_n(0)=Y_n^{'}(0)=0$ $Y_n(b)=Y_n^{"}(b)=0$	$\sin(\lambda x)\left[\cos(\lambda x)-1\right]$	$\sin(\mu y)\left[\cos(\mu y)-1\right]$
CCSS	$X_m(0)=X_m^{'}(0)=0$ $X_m(a)=X_m^{'}(a)=0$	$Y_n(b)=Y_n^{"}(b)=0$ $Y_n(b)=Y_n^{"}(b)=0$	$\sin^2(\lambda x)$	$\sin(\mu y)$
CCCC	$X_m(0)=X_m^{'}(0)=0$ $X_m(a)=X_m^{'}(a)=0$	$Y_n(0)=Y_n^{'}(0)=0$ $Y_n(b)=Y_n^{'}(b)=0$	$\sin^2(\lambda x)$	$\sin^2(\mu y)$
FFCC	$X_m^{"}(0)=X_m^{"'}(0)=0$ $X_m^{"}(a)=X_m^{"'}(a)=0$	$Y_n(0)=Y_n^{'}(0)=0$ $Y_n(b)=Y_n^{'}(b)=0$	$\cos^2(\lambda x)\left[\sin^2(\lambda x)+1\right]$	$\sin^2(\mu y)$
FFSS	$X_m^{"}(0)=X_m^{"'}(0)=0$ $X_m^{"}(a)=X_m^{"'}(a)=0$	$Y_n(b)=Y_n^{"}(b)=0$ $Y_n(b)=Y_n^{"}(b)=0$	$\cos^2(\lambda x)\left[\sin^2(\lambda x)+1\right]$	$\sin(\mu y)$

In which

$$
\begin{aligned}
&S_{11}=A_{11}\psi_{12}+A_{66}\psi_8\\
&S_{12}=(A_{12}+A_{66})\psi_8\\
&S_{13}=-B_{11}\psi_{12}-(B_{12}+2B_{66})\psi_8\\
&S_{14}=(Bs_{12}K_2B+Bs_{66}(K_1A+K_2B))\psi_8+Bs_{11}K_1A\,\psi_{12}\\
&S_{15}=X_{13}\psi_6
\end{aligned}
\tag{33a}
$$

$$
\begin{aligned}
&S_{21}=(A_{12}+A_{66})\psi_{10}\\
&S_{22}=A_{22}\psi_4+A_{66}\psi_{10}\\
&S_{23}=-B_{11}\psi_4-(B_{12}+2B_{66})\psi_{10}\\
&S_{24}=Bs_{22}K_2B\,\psi_4+(Bs_{12}K_1A+Bs_{66}(K_1A+K_2B))\psi_{10}\\
&S_{25}=X_{13}\psi_2
\end{aligned}
\tag{33b}
$$

$$
\begin{aligned}
&S_{31}=B_{11}\psi_{13}+(B_{12}+2B_{66})\psi_{11}\\
&S_{32}=B_{11}\psi_5+(B_{12}+2B_{66})\psi_{11}\\
&S_{33}=-D_{11}\psi_{13}-D_{22}\psi_5-2(D_{12}+2D_{66})\psi_{11}-N_x^0\psi_9-N_y^0\psi_3+\bar{R}_f\\
&S_{34}=Ds_{11}K_1A\psi_{13}+(Ds_{12}+2Ds_{66})(K_1A+K_2B))\psi_{11}\\
&\quad+Ds_{22}K_2B\psi_5\\
&S_{35}=Y_{13}\psi_9+Y_{23}\psi_3-g(z)(N_x^0\psi_9+N_y^0\psi_3)+f'(z)\bar{R}_f
\end{aligned}
\tag{33c}
$$

$$
\begin{aligned}
&S_{41}=-(Bs_{12}K_2B+Bs_{66}(K_1A+K_2B))\,\psi_{11}-Bs_{11}K_1A\,\psi_{13}\\
&S_{42}=-Bs_{22}K_2\psi_5-(Bs_{12}K_1A+Bs_{66}(K_1A+K_2B))\psi_{11}\\
&S_{43}=Ds_{11}K_1A\psi_{13}+(Ds_{12}+2Ds_{66})(K_1A+K_2B))\psi_{11}\\
&\quad+Ds_{22}K_2B\psi_5\\
&S_{44}=-(K_1A)^2Hs_{11}\psi_{13}-Hs_{22}(K_2B)^2\psi_5\\
&\quad-\left(2Hs_{12}K_1AK_2B\right)+Hs_{66}(K_1A+K_2B)^2\psi_{11}\\
&\quad+(As_{44}(K_1A)^2)\psi_9\\
&\quad+(As_{44}(K_2B)^2)\psi_3\\
&S_{45}=(As_{55}K_1A-Y_{13}^sK_1A)\psi_9+(As_{44}K_2B-Y_{23}^sK_2B)\psi_3\\
&S_{55}=As_{55}\psi_1+As_{44}\psi_{11}-Z_{33}\psi_{13}+\left(f'(z)\right)^2\bar{R}_f
\end{aligned}
\tag{33d}
$$

With

$$
\begin{aligned}
&(\psi_i)=\int_0^a\int_0^b\left(X_m^{"}Y_n,X_m^{'}Y_n^{'},X_m^{'}Y_n,X_m^{'}Y_n^{'}\right)dxdy \quad \text{with } i=1,2,3 \text{ and } 4\\
&(\psi_i)=\int_0^a\int_0^b\left(X_m^{"}Y_n^{'},X_mY_n^{"'},X_mY_n^{'}\right)dxdy \quad \text{with } i=5,6 \text{ and } 7\\
&(\psi_i)=\int_0^a\int_0^b\left(X_m^{"}Y_n,X_m^{'}Y_n^{'},X_m^{'}Y_n\right)dxdy \quad \text{with } i=8,9 \text{ and } 10\\
&(\psi_i)=\int_0^a\int_0^b\left(X_mY_n^{"},X_mY_n^{'},X_mY_n\right)dxdy \quad \text{with } i=11,12 \text{ and } 13
\end{aligned}
\tag{34}
$$

The terms S_1,S_2,S_3,L and $\bar{R}_f$ are given by

$$
\begin{aligned}
&\bar{R}_f=L\left[g_1-g_2\left(\psi_{13,xx}+\psi_{13,xy}\right)\right]\\
&S_1=L\left(-p+N^T+N^C\right)\left(\psi_{13,xx}+\psi_{13,xy}\right)\\
&S_2=L\left(-p+N^T+N^C\right)\left(\psi_{13,xx}+\psi_{13,xy}\right)f'(z)\\
&S_2=L\left(-p+N^T+N^C\right)\left(\psi_{13,xx}+\psi_{13,xy}\right)\left(f'(z)\right)^2\\
&L=\left[1-\mu^2\left(\psi_{13,xx}+\psi_{13,xy}\right)\right]
\end{aligned}
\tag{35}
$$

3. Findings and analysis

This section explores the impact of the nonlocal coefficient on the critical buckling temperature of a sandwich Nano-plate made of functionally graded materials (FGM).

3.1 The characteristics of the materials utilised

In the present study, the moisture concentration is specified as β_m=0.440 ($Wt\%\ H_2O$) for the metal component and β_m=0.001 ($Wt\%\ H_2O$) for the ceramic component.

In the current investigation, next dimensionless parameters are considered

$$
T_{cr}=10^{-3}\Delta T_{cr},\ J_1=\frac{K_wa^4}{D_c},\ J_2=\frac{K_pa^2}{D_c},\ D_c=\frac{E_ch^3}{12(1-\nu^2)}
$$

$$
\xi=\frac{H_c}{H_f}
$$

Table 2 The properties of the materials used for FGM nanoplate

Materials	Mechanical proprieties		
	$E\,(GPa)$	$\alpha\,(K^{-1})$	υ
Al	70	$23*10^{-6}$	0.3
Al_2O_3	380	$7*10^{-6}$	0.3

Table 3 The properties of the materials used for a sandwich FGM nanoplate

Materials	Mechanical proprieties		
	$E\,(GPa)$	$\alpha\,(K^{-1})$	υ
Ti 6Al 4V	66.2	$10.6*10^{-6}$	0.3
ZrO2	244.27	$12.776*10^{-6}$	0.3

Table 4 Comparison of nondimensional critical buckling temperature T_{cr} of an FG square plate on elastic foundations under uniform temperature rise

K	Theory	$g_1 = g_2 = 0$			$g_1 = 10,\quad g_2 = 0$			$g_1 = 10,\quad g_2 = 10$		
		a/h			a/h			a/h		
		5	10	20	5	10	20	5	10	20
0	Yaghoobi and Torabi (2013)	5.58069	1.61862	0.42153	5.75623	1.66251	0.43251	9.22123	2.52876	0.64907
	Zenkour and Sobhy (2011)	5.58556	1.61882	0.42154	5.76109	1.66270	0.43252	9.22610	2.52896	0.64908
	Radwan (2019)	5.58394	1.61875	0.42154	5.75948	1.66264	0.43251	9.22448	2.52889	0.64907
	Refrafi *et al.* (2020)	5,56502	1,59416	0,39657	5,74056	1,63804	0,40754	9,20556	2,50429	0,62410
	Present Quasi-3D	**5.88659**	**1.65066**	**0.42522**	**6.06211**	**1.69455**	**0.43616**	**9.52710**	**2.56077**	**0.65276**
1	Yaghoobi and Torabi (2013)	2.67241	0.75845	0.19627	2.83603	0.79935	0.20649	6.06558	1.60674	0.40834
	Zenkour and Sobhy (2011)	2.67174	0.75842	0.19627	2.83535	0.79933	0.20649	6.06491	1.60672	0.40834
	Radwan (2019)	2,64926	0,73358	0,17128	2,81287	0,77449	0,18150	6,04243	1,58188	0,38335
	Present Quasi-3D	**2.86982**	**0.79342**	**0.20361**	**3.03340**	**0.83437**	**0.21382**	**6.26298**	**1.64175**	**0.41563**
5	Yaghoobi and Torabi (2013)	2.35948	0.68678	0.17905	2.58625	0.74347	0.19322	7.06257	1.86255	0.47299
	Zenkour and Sobhy (2011)	2.27131	0.67895	0.17851	2.49808	0.73564	0.19268	6.97440	1.85472	0.47245
	Radwan (2019)	2.27935	0.67972	0.17856	2.50612	0.73641	0.19274	6.98244	1.85549	0.47251
	Refrafi *et al.* (2020)	2,24462	0,65377	0,15350	2,47139	0,71046	0,16767	6,94771	1,82954	0,44744
	Present Quasi-3D	**2.44579**	**0.71583**	**0.18687**	**2.67252**	**0.77257**	**0.20105**	**7.14887**	**1.89164**	**0.48085**
10	Yaghoobi and Torabi (2013)	2.36822	0.70108	0.18373	2.62416	0.76507	0.19972	7.67626	2.02809	0.51548
	Zenkour and Sobhy (2011)	2.27551	0.69254	0.18313	2.53146	0.75653	0.19913	7.58356	2.01955	0.51489
	Radwan (2019)	2.27936	0.69296	0.18316	2.53531	0.75694	0.19916	7.58740	2.01997	0.51492
	Refrafi *et al.* (2020)	2,25119	0,66757	0,15814	2,50713	0,73156	0,17413	7,55922	1,99458	0,48989
	Present Quasi-3D	**2.42085**	**0.72081**	**0.18911**	**2.67681**	**0.78477**	**0.20511**	**7.72887**	**2.04777**	**0.52087**

3.2 Comparative study

To confirm the accuracy of the current formulations, the hygrothermomechanical results of the nanoplates made of functionally graded materials were compared with those determined by Yaghoobi and Torabi (2013), Zenkour and Sobhy (2011), Radwan (2019), Refrafi *et al.* (2020).

Table 4 presents the 2D and 3D results obtained for the critical buckling temperature (Tcr) under a uniform temperature rise in a simply supported functionally graded (FG) plate, with and without Winkler-Pasternak elastic foundations. These results are compared to those from Yaghoobi and Yaghoobi and Torabi (2013), who used the First-Order Plate Theory (FPT), Zenkour and Sobhy (2011) who applied the Third-Order Plate Theory (TPT), Radwan (2019), and Refrafi *et al.* (2020). In this comparison, various values were used for the inhomogeneity parameter (k) and side-to-thickness ratio (a/h). The results strongly correlate with those of prior studies using the 2D model across all examined parameter values. They revealed that elastic foundations increase the critical buckling temperature, which decreases with higher values of the

Table 5 Comparison of nondimensional critical buckling temperature Tcr of FG sandwich square plates under nonlinear temperature rise (γ=5)

ξ	K	Theory	a/h				
			5	10	15	25	50
0	0.5	Zenkour and Sobhy (2011)	21.61337	5.90995	2.58239	0.81982	0.06380
		Radwan (2019)	21.60648	5.90948	2.58230	0.81981	0.06380
		Refrafi *et al*. (2020)	21.60480	5.90938	2.58228	0.81981	0.06380
		Present Quasi-3D	**22.92219**	**6.03878**	**2.61685**	**0.82765**	**0.06525**
	2	Zenkour and Sobhy (2011)	23.02926	6.12449	2.64800	0.82107	0.04052
		Radwan (2019)	23.00135	6.12245	2.64759	0.82102	0.04051
		Refrafi *et al*. (2020)	22.98800	6.12147	2.64739	0.82100	0.04050
		Present Quasi-3D	**24.45545**	**6.26160**	**2.68529**	**0.82983**	**0.04223**
0.5	0.5	Zenkour and Sobhy (2011)	21.33821	5.83566	2.54875	0.80744	0.06048
		Radwan (2019)	21.33354	5.83536	2.54869	0.80743	0.06048
		Refrafi *et al*. (2020)	21.33300	5.83535	2.54869	0.80743	0.06048
		Present Quasi-3D	**22.63650**	**5.96344**	**2.58287**	**0.81517**	**0.06194**
	2	Zenkour and Sobhy (2011)	22.35275	5.89838	2.53488	0.77011	0.01668
		Radwan (2019)	22.33166	5.89686	2.53458	0.77007	0.01668
		Refrafi *et al*. (2020)	22.32160	5.89614	2.53443	0.77005	0.01668
		Present Quasi-3D	**23.79307**	**6.03565**	**2.57213**	**0.77890**	**0.01835**
1	0.5	Zenkour and Sobhy (2011)	21.12437	5.79091	2.53084	0.80247	0.06078
		Radwan (2019)	21.12333	5.79089	2.53084	0.80246	0.06078
		Refrafi *et al*. (2020)	21.12500	5.79100	2.53090	0.80247	0.06079
		Present Quasi-3D	**22.41257**	**5.91799**	**2.56473**	**0.81015**	**0.06213**
	2	Zenkour and Sobhy (2011)	21.98303	5.81247	2.49756	0.75699	0.01363
		Radwan (2019)	21.97101	5.81161	2.49738	0.75698	0.01363
		Refrafi *et al*. (2020)	21.96600	5.81120	2.49730	0.75697	0.01363
		Present Quasi-3D	**23.43233**	**5.95050**	**2.53485**	**0.76571**	**0.01532**
2	0.5	Zenkour and Sobhy (2011)	20.80375	5.73532	2.51144	0.79933	0.06402
		Radwan (2019)	20.80829	5.73575	2.51152	0.79935	0.06403
		Refrafi *et al*. (2020)	20.81300	5.73610	2.51160	0.79936	0.06403
		Present Quasi-3D	**22.06965**	**5.86085**	**2.54483**	**0.80683**	**0.06533**
	2	Zenkour and Sobhy (2011)	21.54679	5.75368	2.48202	0.75946	0.02279
		Radwan (2019)	21.54827	5.75383	2.48206	0.75946	0.02279
		Refrafi *et al*. (2020)	21.55000	5.75400	2.48210	0.75947	0.02279
		Present Quasi-3D	**22.98484**	**5.89054**	**2.51844**	**0.76782**	**0.02434**

inhomogeneity parameter (k) or the side-to-thickness ratio (a/h). Notably, the critical buckling temperature in the 3D model surpasses that of the 2D model owing to the influence of stretching effects.

Table 5 provides a comparison of the critical buckling temperature change (Tcr) in functionally graded (FG) sandwich plates, considering the non-linear temperature effect (γ=5), the inhomogeneity parameter (k), the side-to-thickness ratio (a/h) and the core-to-face thickness ratio (ξ). The results obtained are compared with those of Zenkour and Sobhy (2011), Radwan (2019), and Refrafi *et al*. (2020) and the findings confirm the validity of this comparison. Here, our analysis reveals that the critical buckling temperature diminishes as the core-to-face thickness ratio (ξ) or the side-to-thickness ratio (a/h) increases, primarily due to reduced structural stiffness and enhanced susceptibility to thermal deformation in thicker cores or thinner plates relative to their lateral dimensions. Conversely, the critical buckling temperature rises with an increase in the inhomogeneity parameter (k) under nonlinear temperature effects, as greater material gradation enhances thermal resistance and stiffness distribution across the FG nanoplate, thereby improving stability against buckling.

Table 6 presents the results obtained using both the 2D and 3D models, verified by comparison with those reported by Zenkour and Sobhy (2011). These results include data for a simply supported nanoplate, whether it is freestanding or supported on an elastic foundation. The analysis considered the aspect ratio (b/a), side-to-thickness ratio (a/h), and nonlocal parameter (μ) of the plate. The findings indicate that the critical buckling temperature decreases as the side-to-thickness ratio (a/h) or nonlocal parameter (μ) increases. Conversely, it increased with higher values of the elastic foundation parameters (g1 and g2). Furthermore, the aspect ratio (b/a) also affected the critical buckling temperature; as the aspect ratio (b/a) increased, the critical buckling temperature decreased. However, this effect diminishes in the presence of an elastic foundation and nonlocal parameter (μ).

3.3 Parametric study

Table 6 Comparison of the non-dimensional critical buckling temperature Tcr of an FGM nanoplate without or resting on elastic foundations

g_1	g_2	μ	b/a	T_{cr}								
				a/h=5			a/h=10			a/h=50		
				Zenkour and Sobhy (2011)	Present 2D	**Present Quasi-3D**	Zenkour and Sobhy (2011)	Present 2D	**Present Quasi-3D**	Zenkour and Sobhy (2011)	Present 2D	**Present Quasi-3D**
			1	41.33314	41.32890	**43.56079**	11.97928	11.97952	**12.21488**	0.50502	0.50498	**0.50774**
		0	2	27.73639	27.73612	**28.80574**	7.63958	7.63976	**7.74898**	0.31591	0.31586	**0.31752**
			3	24.99608	24.99612	**25.87944**	6.81646	6.81659	**6.90715**	0.28085	0.28084	**0.28230**
			1	5.27870	5.27811	**5.56319**	4.42441	4.42453	**4.51141**	0.47275	0.47270	**0.47529**
0	0	1	2	5.26422	5.26414	**5.46720**	3.69560	3.69542	**3.74854**	0.30296	0.30293	**0.30452**
			3	5.21345	5.21345	**5.39764**	3.49807	3.49814	**3.54461**	0.27058	0.27057	**0.27196**
			1	0.66163	0.66157	**0.69723**	0.73186	0.73190	**0.74629**	0.31276	0.31275	**0.31443**
		3	2	0.70360	0.70360	**0.73070**	0.72036	0.72040	**0.73065**	0.22822	0.22821	**0.22939**
			3	0.71111	0.71113	**0.73620**	0.71469	0.71471	**0.72421**	0.20935	0.20935	**0.21043**
			1	54.32305	54.31875	**56.55063**	15.22676	15.22700	**15.46234**	0.63492	0.63483	**0.63764**
		0	2	48.52024	48.51997	**49.58952**	12.83554	12.83568	**12.94498**	0.52373	0.52371	**0.52538**
			3	48.37790	48.37794	**49.26125**	12.66192	12.66203	**12.75261**	0.51469	0.51463	**0.51614**
			1	18.26859	18.26805	**18.55308**	7.67188	7.67195	**7.75883**	0.60265	0.60260	**0.60519**
100	0	1	2	26.04804	26.04796	**26.25097**	8.89152	8.89169	**8.94297**	0.51079	0.51080	**0.51235**
			3	28.59525	28.59528	**28.77950**	9.34352	9.34361	**9.39008**	0.50441	0.50440	**0.50584**
			1	13.65153	13.65146	**13.68720**	3.97936	3.97934	**3.99371**	0.44265	0.44262	**0.44432**
		3	2	21.48743	21.48742	**21.51459**	5.91632	5.91633	**5.92667**	0.43605	0.43605	**0.43725**
			3	24.09292	24.09293	**24.11806**	6.56010	6.56017	**6.56970**	0.44318	0.44318	**0.44427**
			1	79.96407	79.95974	**82.19165**	21.63702	21.63723	**21.87261**	0.89134	0.89126	**0.89399**
		0	2	74.16127	74.16102	**75.23055**	19.24580	19.24592	**19.35525**	0.78016	0.78011	**0.78174**
			3	74.01893	74.01894	**74.90228**	19.07217	19.07230	**19.16288**	0.77109	0.77108	**0.77263**
			1	43.90961	43.90905	**44.19412**	14.08213	14.08223	**14.16914**	0.85905	0.85892	**0.86158**
100	10	1	2	51.68907	51.68898	**1.89206**	15.30181	15.30187	**15.35473**	0.76720	0.76708	**0.76879**
			3	54.23630	54.23629	**54.42055**	15.75378	15.75385	**15.80032**	0.76085	0.76079	**0.76227**
			1	39.29257	39.29248	**39.32825**	10.38960	10.38962	**10.40400**	0.69905	0.69904	**0.70062**
		3	2	47.12846	47.12845	**47.15560**	12.32659	12.32660	**12.33691**	0.69247	0.69247	**0.69364**
			3	49.73397	49.73394	**49.75906**	12.97039	12.97041	**12.97990**	0.69958	0.69963	**0.70068**

In this subsection, the influence of the nonlocal parameter μ, moisture concentration ΔC aspect ratio (a/b), and side-to-thickness ratio (a/h) on hygro-thermomechanical buckling are presented in tabular form (7 & 8) and analysed graphically in Figs. (2-8).

Table 7 illustrates the influence of the nonlocal parameter (μ), varying moisture content (ΔC %), and core-to-face thickness ratio (ξ) on the critical buckling temperature of FG sandwich plates under uniform, linear, and nonlinear hygrothermal loads. Physically, an increase in the moisture content (ΔC %) reduces the critical buckling temperature owing to material softening and increased hygroscopic expansion. Similarly, a higher nonlocal parameter (μ) lowers the stiffness through size-dependent effects, thereby decreasing the buckling temperature across all load types. Additionally, the hygrothermal load type impacts stability: uniform loads yield the lowest critical temperatures owing to consistent stress distribution, whereas nonlinear loads with uneven stress gradients result in the highest critical temperatures, enhancing thermal resistance.

Table 8 details the critical buckling temperature for a simply supported functionally graded (FG) nanoplate under a linear temperature rise (γ=1), analysing the impact of the aspect ratio (b/a), side-to-thickness ratio (a/h), and nonlocal parameter (μ). Physically, an increase in a/h lowers the critical buckling temperature owing to the reduced structural stiffness of the thinner plates relative to their width. Similarly, a higher μ decreases the stiffness through size-dependent effects, thereby reducing the buckling temperature. Initially, increasing b/a lowers the critical temperature owing to the altered load distribution; however, the stabilising effect of the elastic foundation and nonlocal interactions causes it to increase with a further b/a increase, enhancing the thermal resistance.

3.4 Graphical illustrations

After analysing and interpreting the results presented in the tables, it is essential to complete this study by examining the tendencies and overall behaviours through the curves. These graphs provide a visual representation of the relationships between the studied variables, allowing the identification of patterns, critical points, and asymptotes that are not always evident in raw data. This step aims to deepen the understanding of the phenomena by highlighting

Table 7 Hygrothermal effects on critical buckling Tcr of FG sandwich square plates under various types of hygrothermal rise and various types of moisture distributions for various values of the core-to-thickness ratio

		Uniform hygrothermal			Linear hygrothermal			Non-linear hygrothermal		
		μ			μ			μ		
ξ	$\Delta C\%$	0	2	4	0	2	4	0	2	4
0	0.01	22.0007	17.8701	14.8901	45.3550	37.0938	31.1342	76.1779	62.4971	52.6260
	0.03	18.0167	13.8861	10.9061	41.3710	33.1100	27.1502	71.7074	58.0263	48.1558
	0.05	14.0326	9.90219	6.92215	37.3866	29.1260	23.1663	67.2374	53.5561	43.6854
0.5	0.01	19.0543	15.3069	12.6036	38.7613	31.2666	25.8597	65.6347	53.0620	43.9904
	0.03	16.4725	12.7251	10.0218	36.1795	28.6847	23.2779	62.5177	49.9449	40.8738
	0.05	13.8907	10.1433	7.43985	33.5978	26.1030	20.6961	59.4011	46.8279	37.7568
1	0.01	17.9527	14.2520	11.5821	36.2225	28.8210	23.4810	61.0549	48.6590	39.7166
	0.03	16.0430	12.3423	9.67238	34.3128	26.9111	21.5712	58.6438	46.2480	37.3056
	0.05	14.1334	10.4326	7.76270	32.4030	25.0013	19.6617	56.2327	43.8365	34.8945
2	0.01	17.3042	13.4621	10.6903	34.5982	26.9139	21.3703	57.4119	44.7060	35.5395
	0.03	16.0484	12.2062	9.43442	33.3425	25.6577	20.1145	55.7426	43.0374	33.8701
	0.05	14.7925	10.9504	8.17853	32.0868	24.4018	18.8584	54.0737	41.3682	32.2013

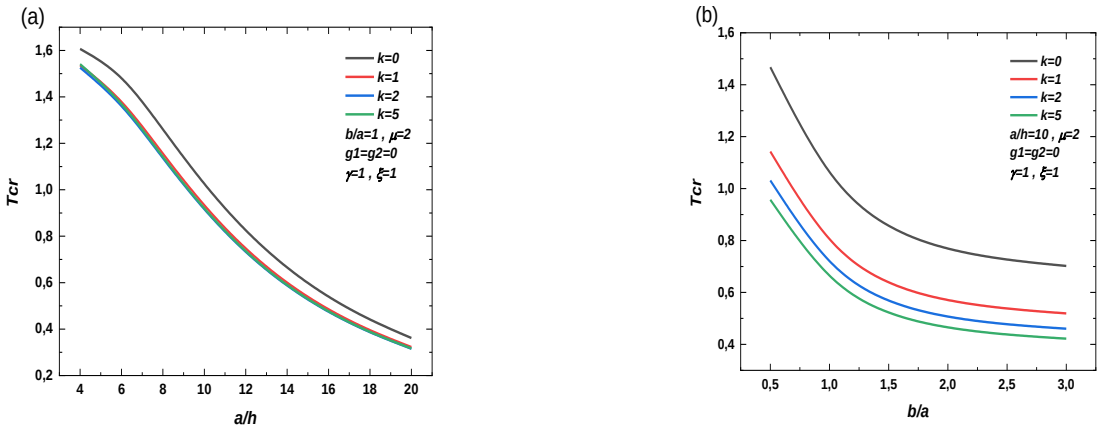

Fig. 2 Buckling temperature change (Tcr) of FG sandwich nanoplate under linear temperature rise (γ= 1) vs. (a) the side-tc thickness ratio (a/h) and (b) plate aspect ratio (b/a) for various values of the power law index (k)

the key interactions and dependencies between the parameters. Thus, the analysis of the curves provides additional insights to validate the formulated hypotheses and guide the conclusions of this study.

Fig. 2 illustrates the influence of the power law index (k) on the critical buckling temperature of 3D functionally graded (FG) sandwich nanoplates without Winkler-Pasternak elastic foundations, with a nonlocal parameter (μ=2) and linear temperature effect (γ=1). The critical buckling temperature decreases as the side-to-thickness ratio (a/h) (curve (a)) and aspect ratio (b/a) (curve (b)) increase owing to the reduced bending stiffness in thinner or wider plates. The proximity of the curves reflects the nonlocal parameter (μ) that influences the thickness effects (curve (a)). Additionally, the critical buckling temperature (Tcr) decreases with a higher power law index (k) as the material properties shift toward metal, which exhibits lower thermal resistance compared to ceramic, thus reducing thermal stability.

Fig. 3 depicts the variation in the critical buckling temperature (Tcr) of a 3D functionally graded material (FGM) nanoplate with respect to the side-to-thickness ratio (a/h) under the influence of Winkler-Pasternak elastic foundations, with each parameter analysed separately. Physically, Tcr decreases as a/h increases owing to the reduced bending stiffness of thinner plates relative to their lateral dimensions, making them more susceptible to buckling under thermal loads. Conversely, Tcr increases with higher elastic foundation parameters (g1 or g2) because they enhance the structural support and resistance to deformation. Notably, the Pasternak parameter (g2), which accounts for shear interactions, has a more pronounced effect on increasing Tcr than the Winkler parameter (g1), which only provides normal stiffness.

Fig. 4 illustrates the change in the critical buckling temperature of FG sandwich plates as a function of the side-to-thickness ratio (a/h), influenced by the core-to-thickness ratio (ξ), Winkler-Pasternak elastic foundations, nonlocal

Table 8 Effects of plate aspect ratio, side-to-thickness ratio, and nonlocal parameter on critical buckling temperature Tcr of SS nanoplate under linear temperature rise

		T_{cr}				
b/a	*a/h*	*μ=0*	*μ=1*	*μ=2*	*μ=3*	*μ=4*
0.5	5	74.46252	68.43561	66.40290	65.86614	65.66088
	10	18.90098	17.92825	16.94696	16.49809	16.28800
	15	8.18502	7.93660	7.53975	7.26850	7.11049
	20	4.39262	4.30566	4.13099	3.97597	3.86701
	25	2.62937	2.59198	2.50665	2.41693	2.34396
1	5	71.79972	69.83449	68.41664	67.89497	67.67210
	10	17.69603	17.49027	17.14534	16.89742	16.74803
	15	7.58959	7.54373	7.44227	7.33929	7.25837
	20	4.04503	4.02989	3.99198	3.94611	3.90313
	25	2.40310	2.39676	2.37993	2.35739	2.33375
2	5	72.25275	71.28007	70.29869	69.84983	69.63979
	10	17.73055	17.64359	17.46890	17.31393	17.20495
	15	7.59749	7.57889	7.53320	7.47955	7.43070
	20	4.04791	4.04184	4.02573	4.00405	3.98123
	25	2.40451	2.40198	2.39503	2.38496	2.37342
3	5	72.60804	71.80163	70.92345	70.49789	70.29319
	10	17.80812	17.73839	17.59293	17.45753	17.35856
	15	7.63092	7.61618	7.57906	7.53403	7.49176
	20	4.06652	4.06179	4.04879	4.03106	4.01180
	25	2.41635	2.41436	2.40882	2.40068	2.39113

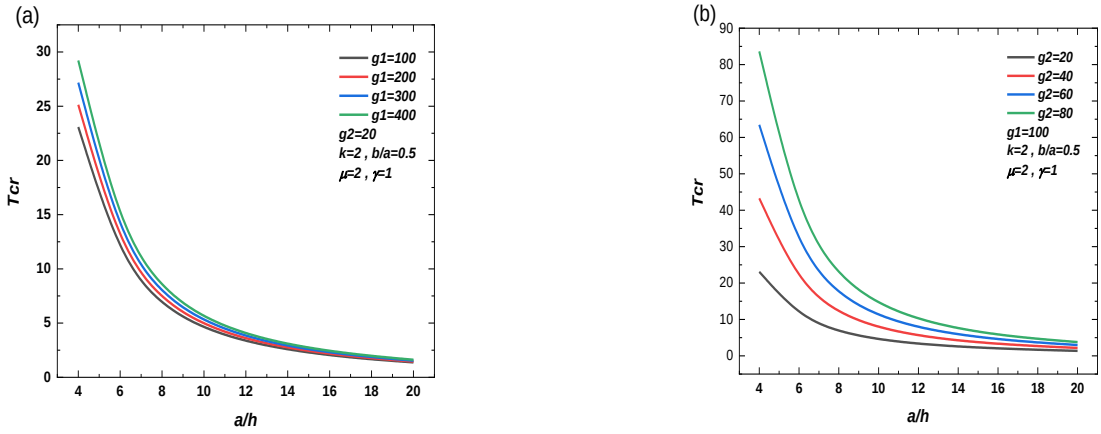

Fig. 3 Effects of (a) Winkler parameter (g1) and (b) shear layer parameter (g2) on critical buckling temperature (Tcr) of SSS nanoplate

parameter (μ), and nonlinear Fourier temperature distribution (γ). In general, it can be observed that as the side-to-thickness ratio (a/h) increases, the critical buckling temperature (Tcr) decreases. Additionally, it is noted that the critical buckling temperature is reduced when moisture is present compared with conditions without moisture. Furthermore, the core–outer thickness ratio (ξ) significantly affects the critical buckling temperature (Tcr); as (ξ) increases, the critical buckling temperature also decreases. As shown in Fig. 5, the critical buckling temperature increased as the aspect ratio (b/a) increased, contrary to what is typically expected. This is owing to the effect of the elastic foundations and the nonlocal parameter (μ), which counteracts the influence of the aspect ratio (b/a).

Fig. 5(a) highlights the variation in the critical buckling temperature (Tcr) with the side-to-thickness ratio (a/h) for a simply supported FG nanoplate under uniform (γ=0), linear (γ=1), and nonlinear (γ=2,3) temperature distributions. For all cases, Tcr decreased as a/h increased, reflecting the reduced stiffness in thinner plates. Nonlinear temperature distributions result in a higher Tcr than linear and uniform distributions, indicating greater thermal stability. Uniform temperature yields the lowest Tcr owing to uniformly destabilising thermal stresses. Including the Winkler and Pasternak elastic foundations enhances stability by increasing stiffness, and these effects persist across all temperature profiles. At a higher a/h, the curves for

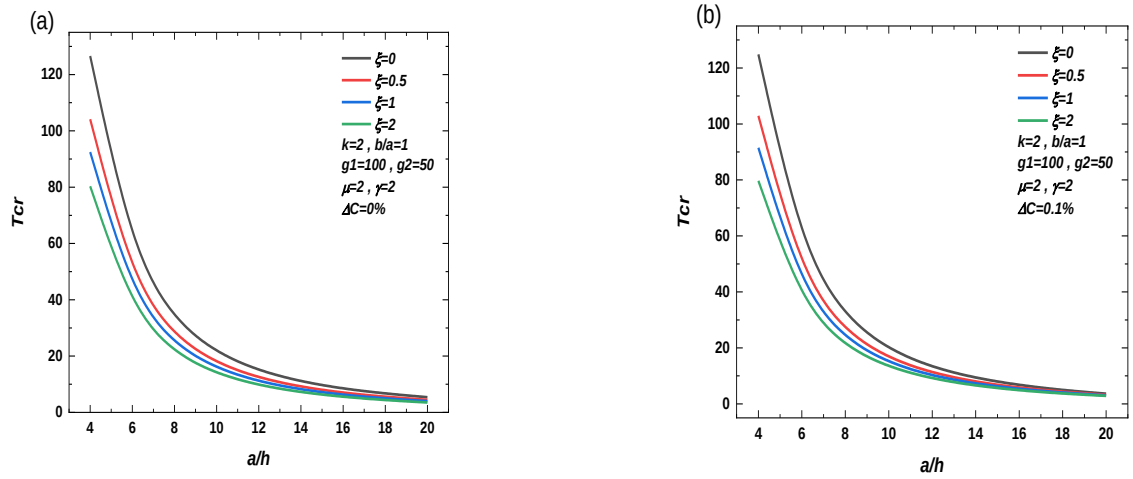

Fig. 4 Buckling temperature change Tcr of FG sandwich nanoplate under non-linear temperature rise vs. the side-to-thickness ratio (a/h) and (a) thermal buckling and (b) hygrothermal buckling for various values of the core-to-face thickness ratio (ξ)

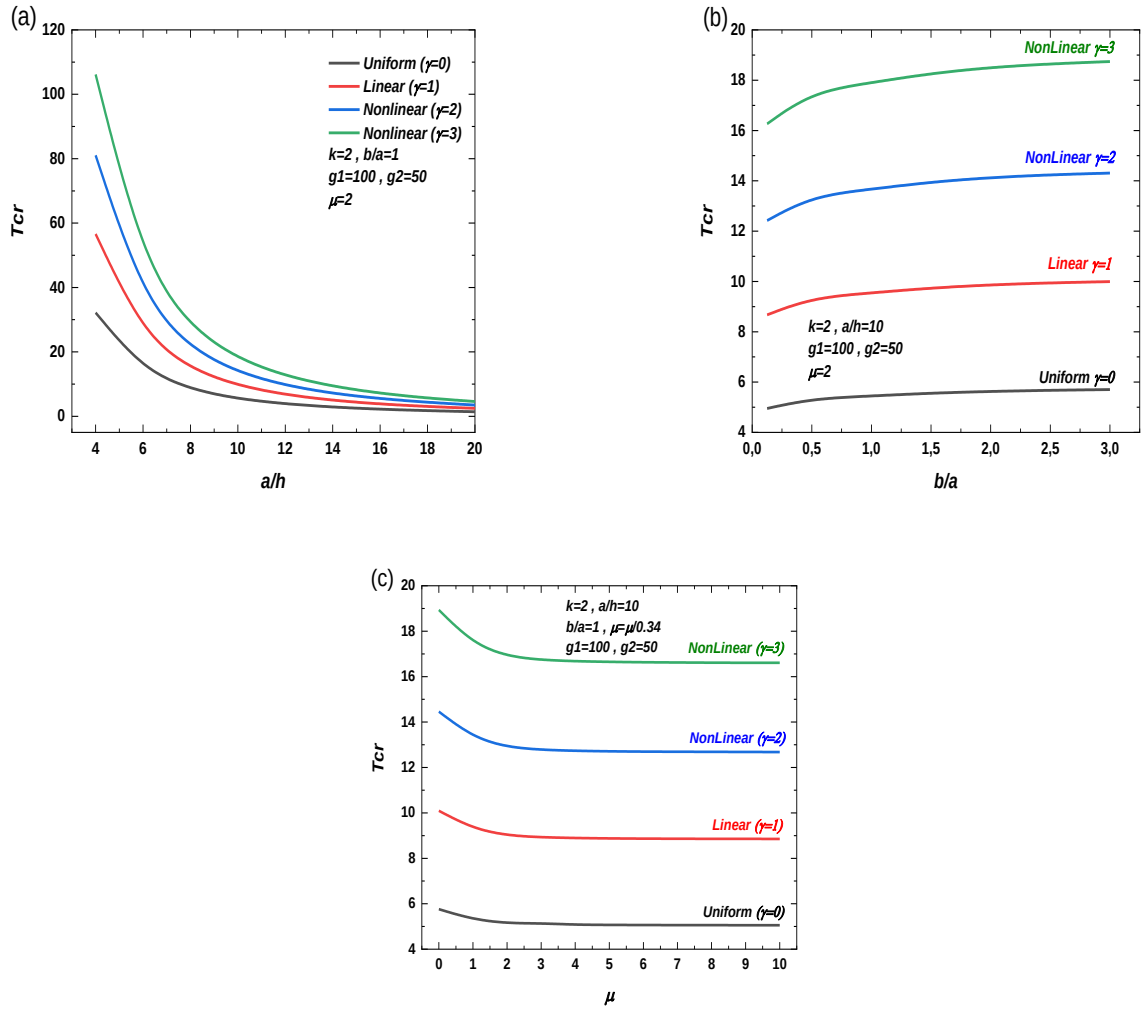

Fig. 5 Effects of (a) side-to-thickness ratio(a/h), (b) plate aspect ratio (b/a) and (c) nonlocal parameter (μ) on critical buckling temperature (Tcr) of SSSS nanoplate due to uniform, linear and non-linear temperature rise

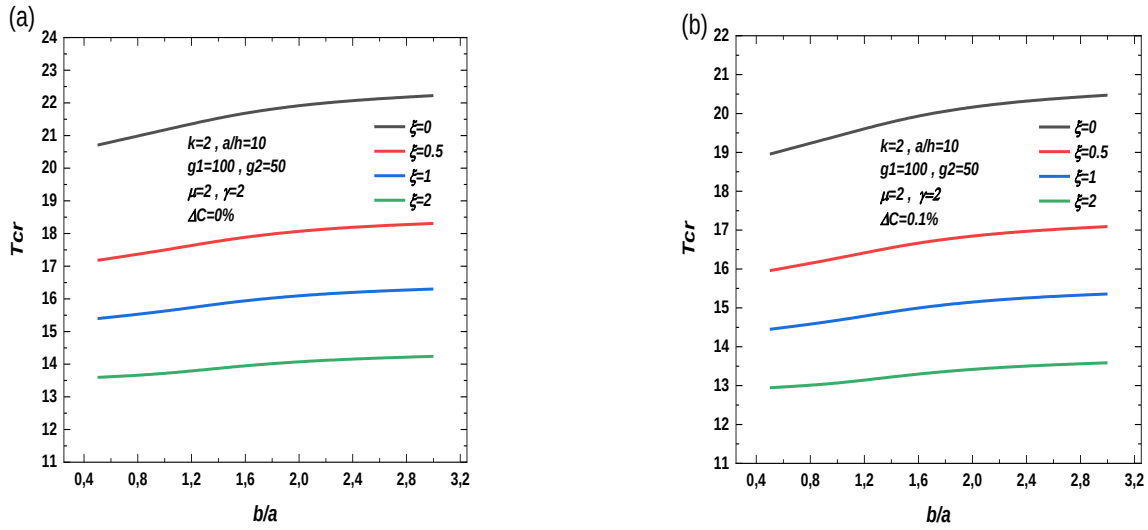

Fig. 6 Buckling temperature change (Tcr) of FG sandwich nanoplate under non-linear temperature rise vs. plate aspect rati (b/a), (a) thermal buckling and (b) hygrothermal buckling for various values of the core-to-face thickness ratio (ξ)

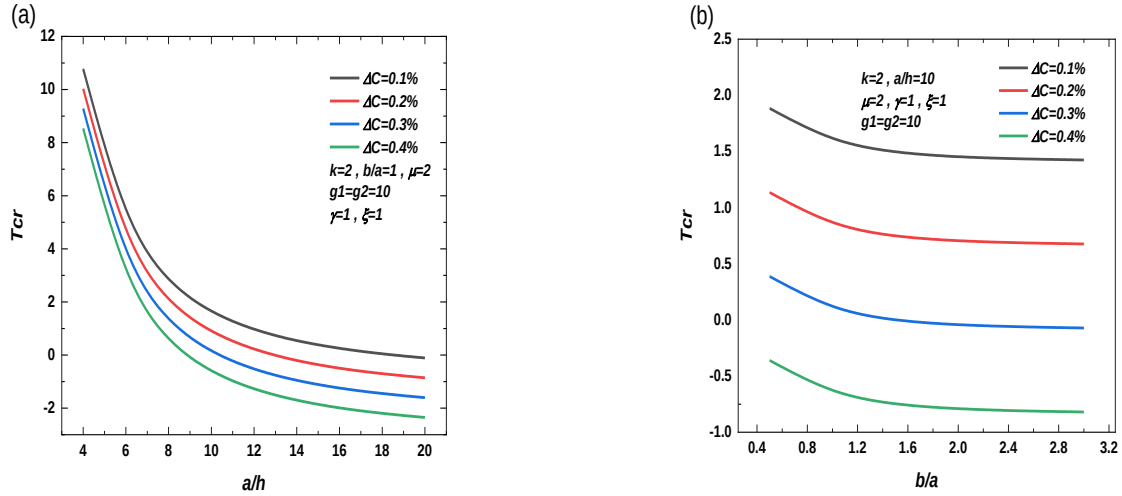

Fig. 7 Effect of the moisture concentration (ΔC) on the buckling temperature (Tcr) of FG sandwich nanoplate resting on elastic foundations vs. (a) the side-to-thickness (a/h) and (b) plate aspect ratio (b/a)

different temperature distributions converge, indicating that geometry dominates over other factors for thinner plates. These results underline the importance of the temperature profiles, foundation stiffness, and geometry in the design of thermally stable FG nanoplates. Fig. 5(b) illustrates the influence of the plate aspect ratio (b/a) on the critical buckling temperature (Tcr) of a simply supported FG nanoplate subjected to uniform, linear, and nonlinear temperature rises. The results showed that Tcr increased with the plate aspect ratio (b/a) across all thermal loading cases. A uniform temperature rise (γ=0) yields the lowest (Tcr), whereas nonlinear temperature distributions (γ=2,3) result in significantly higher (Tcr), indicating enhanced thermal stability. The effect of the temperature gradient is more pronounced in nonlinear cases, with higher γ values indicating a larger increase in (Tcr). Fig. 5(c) shows the effect of the nonlocal parameter (μ) on the critical buckling temperature (Tcr) of a simply supported square functionally graded (FG) nanoplate under uniform, linear, and nonlinear temperature distributions. The results indicate that (Tcr) decreases as μ increases, signifying a reduction in thermal stability with higher nonlocal effects. Uniform temperature rise (γ=0) shows the lowest (Tcr), while nonlinear temperature distributions (γ=2,3) exhibit higher (Tcr), reflecting the stabilising effect of nonlinear gradients. Among the nonlinear cases, (γ=3) provided the highest (Tcr). This trend highlights that as nonlocal effects become more significant (μ>0), their influence on reducing Tcr is more pronounced, particularly for higher γ values.

Fig. 6 illustrates the variation in the buckling

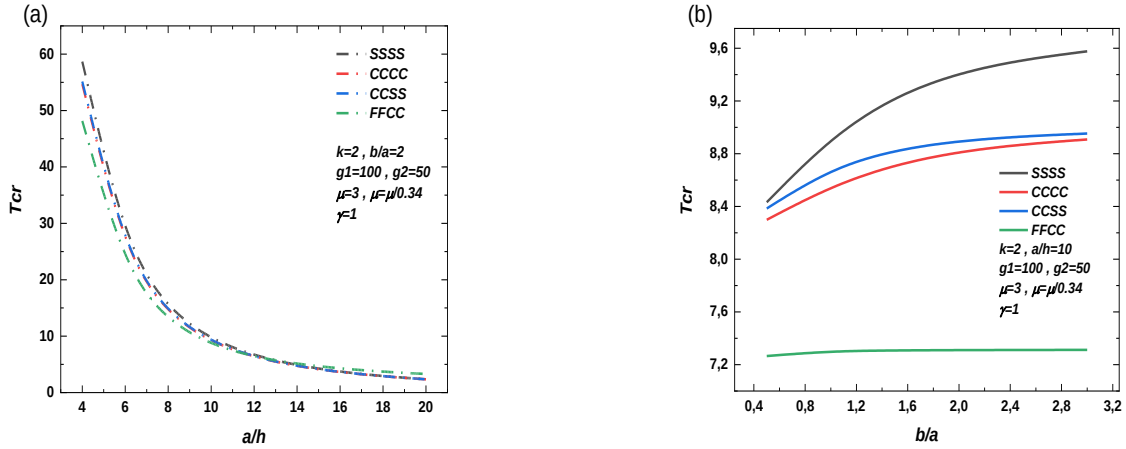

Fig. 8 Critical buckling temperature (Tcr) of nanoplate for various boundary conditions vs. (a) side-to-thickness ratio (a/h) and (b) plate aspect ratio (b/a) under linear temperature change

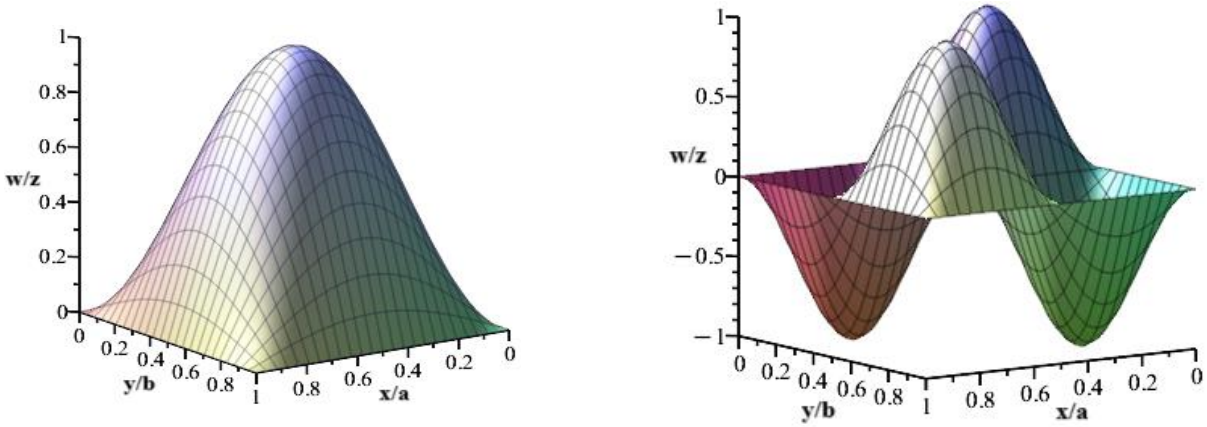

Fig. 9 Pattern of mode shapes of simply supported (SSSS) FG nanoplates: (a) for the 1st mode (m=1, n=1), and (b) for the 2nd mode (m=2, n=2)

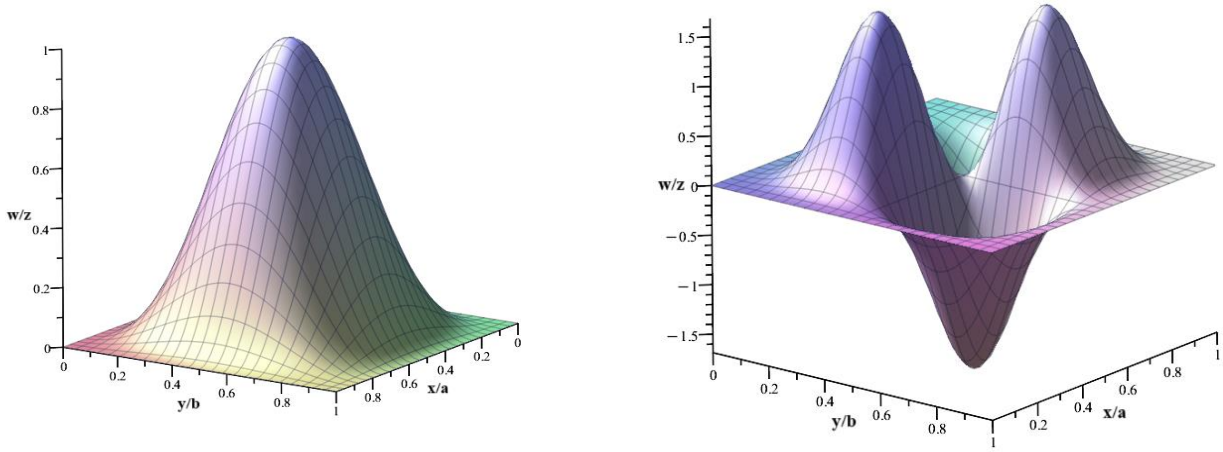

Fig. 10 Pattern of mode shapes of clamped (CCCC) FG nanoplates: (a) for the 1st mode (m=1, n=1), and (b) for the 2nd mode (m=2, n=2)

temperature (Tcr) of functionally graded sandwich nanoplates under thermal and hygrothermal loading as a function of the aspect ratio (b/a). Thermal buckling (Fig. 6(a)), Tcr decreases with increasing b/a owing to the reduced structural stiffness in the wider plates, making them more susceptible to buckling under thermal stress. When

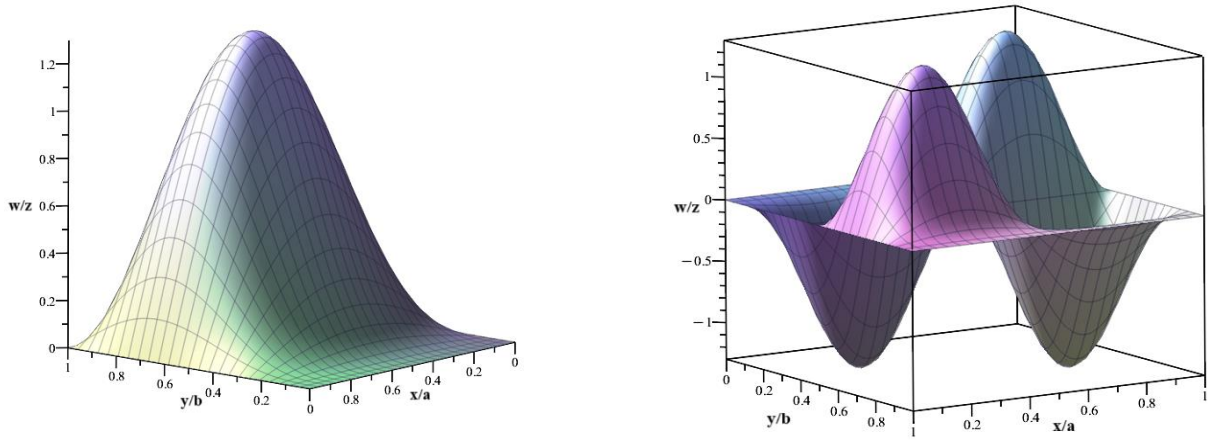

Fig. 11 Pattern of mode shapes of clamped-simply supported (CSSS) FG nanoplates: (a) for the 1st mode (m=1, n=1), and (b) for the 2nd mode (m=2, n=2)

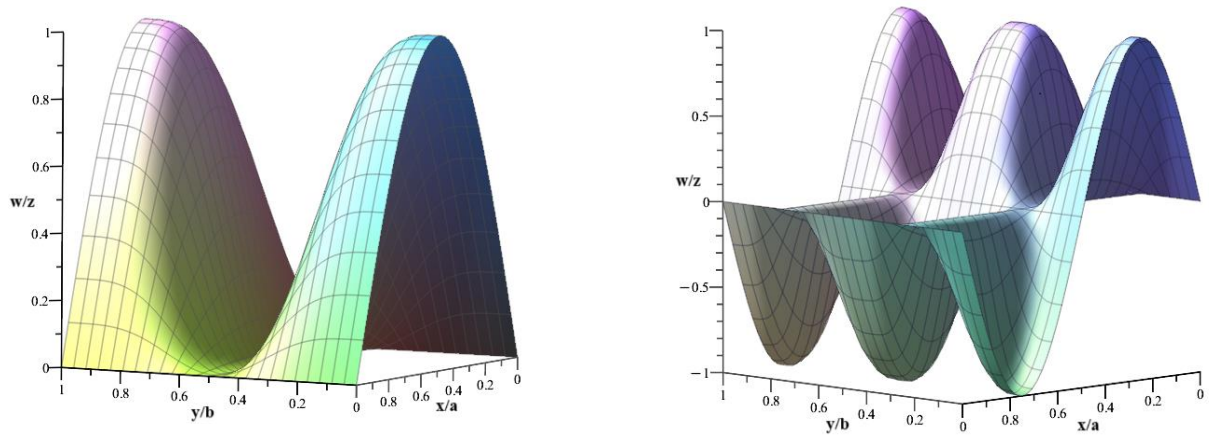

Fig. 12 Pattern of mode shapes of free-simply supported (FFSS) FG nanoplates: (a) for the 1st mode (m=1, n=1), and (b) for the 2nd mode (m=2, n=2)

the effects of moisture were considered (Fig. 6(b), hygrothermal buckling), Tcr drops further compared to thermal buckling, as moisture (ΔC) induces material softening and hygroscopic expansion, exacerbating instability. The core–outer thickness ratio (ξ) also plays a critical role: a higher ξ (thicker core) typically enhances stiffness and elevates Tcr, whereas a thinner core diminishes stability. This study highlights that the aspect ratio, moisture content, and material parameters significantly influence the buckling behaviour of FG nanoplates, with hygrothermal loading causing greater destabilisation than pure thermal loading owing to the combined thermal and moisture-induced stresses.

Fig. 7 shows the impact of moisture content (ΔC) on the critical buckling temperature (Tcr) of a functionally graded (FG) sandwich nanoplate, considering the influence of an elastic foundation, linear thermal rise (γ=1), and nonlocal parameter (μ). The effect was analysed with respect to (a) the side-to-thickness ratio (a/h) and (b) the plate aspect ratio (b/a). An increase in moisture (ΔC) reduces Tcr owing to material softening and hygroscopic expansion, which weaken the structural integrity and lower the resistance of the plate to thermal buckling under combined environmental loads.

Fig. 8 illustrates the effect of various boundary conditions on the critical buckling temperature (T_{cr}) of a nanoplate resting on an elastic foundation, with a nonlocal parameter μ=3. The figure shows this effect in terms of the (a) side-to-thickness ratio and (b) plate aspect ratio. It is observed that under a linear thermal load ($\gamma = 1$), the critical buckling temperature (T_{cr}) decreases with an increase in the side-to-thickness ratio (a/h) and increases with an increase in the plate aspect ratio (b/a). Typically, the critical buckling temperature decreases with increasing aspect ratio, with the highest buckling temperature occurring for plates with FFCC boundary conditions and the lowest for plates with SSSS boundary conditions. However, owing to the influence of the elastic foundation and the nonlocal parameter, the opposite behaviour is observed; this means that the critical buckling temperature is affected by the boundary conditions.

To help readers grasp the manifestation of instability under various loading and boundary conditions, Figs. 9-12 illustrate the mode shape distributions of rectangular FG nanoplates for different supports and two deformation modes.

4. Conclusions

The hygro-thermomechanical buckling behaviour of simply supported FG nanoplates resting on Winkler–Pasternak foundations was studied using the quasi-3D approach. This approach employs quasi-3D theory, incorporating five unknown terms. Eringen's theory for nonlocal integral elasticity, combined with the nano-size effect, is utilised to formulate the equilibrium and stability equations. The principle of virtual work is applied to derive these equations, and the stability equations are determined based on the neighbouring equilibrium criterion. The Navier solution method was adopted to solve the stability equation system for various boundary conditions. The proposed model was validated by comparing it with existing models in the literature. The effects of different parameters are analysed, and the findings are summarised in several key points:

- The critical buckling temperature (Tcr) decreased with an increase in the side-to-thickness ratio (a/h) and increased with an increase in the elastic foundation parameters (g1) or (g2).
- The critical buckling temperature of the nanoplate under the influence of a uniform temperature rise has the lowest value. At the same time, it was intermediate in the case of linear temperature rise and reached its highest value in the case of nonlinear temperature rise.
- The critical buckling temperature is reduced when moisture is present compared with conditions without moisture.
- The critical buckling temperature increases as the aspect ratio (b/a) increases owing to the effect of the elastic foundations and the nonlocal parameter (μ).
- The critical buckling temperature is affected by the boundary conditions.

This study showed that increasing the nonlocal parameter reduces the nanoplate stiffness and lowers the critical buckling loads, whereas a stiffer shear foundation mitigates this effect and enhances the structural stability. Building on these findings, future research could focus on experimental validation through micro- and nanoscale testing to confirm theoretical predictions. Extending the current work to dynamic instability analysis would also be valuable in understanding how time-dependent influences the buckling behaviour in nonlocal elastic systems. Moreover, incorporating thermomechanical coupling can shed light on the impact of temperature gradients and thermal stresses, which are particularly relevant in operational environments. Finally, investigating heterogeneous and composite nanoplate systems, such as functionally graded or multilayered structures, may offer effective strategies to tailor the stiffness and enhance the buckling resistance under complex loading conditions.

Acknowledgments

The author(s) received no financial support for the research, authorship, and/or publication of this article.

References

Abouelregal, A., Mohammed, W. and Mohammad-Sedighi, H. (2021), "Vibration analysis of functionally graded microbeam under initial stress via a generalized thermoelastic model with dual-phase lags", *Arch. Appl. Mech.*, **91**, 2127-2142. https://doi.org/10.1007/s00419-020-01873-2.

Baghdali, I., Attia, A., Bourada, F., Bousahla, A., Tounsi, A., Heireche, H., Tounsi, A., Bourada, M. and Yaylaci, M. (2025), "Analysis of the impact of the viscoelastic foundation on bending and vibration of FG porous nanoplates within integral higher-order shear deformation theory", *Phys. Mesomech.*, **28**(2), 245-262. https://doi.org/10.1134/S1029959924601313.

Beg, M.S. and Yasin, M.Y. (2021), "Bending, free and forced vibration of functionally graded deep curved beams in thermal environment using an efficient layerwise theory", *Mech. Mater.*, **159**, 103919. https://doi.org/10.1016/j.mechmat.2021.103919.

Berkia, A., Benguediab, S., Menasria, A., Bouhadra, A., Bourada, F., Mamen, B., Tounsi, A., Benrahou, K.H., Benguediab, M. and Hussain, M. (2022), "Static buckling analysis of bi-directional functionally graded sandwich (BFGSW) beams with two different boundary conditions", *Steel Compos. Struct.*, **44**(4), 503-517. https://doi.org/10.12989/scs.2022.44.4.503.

Bouhadra, A., Menasria, A. and Rachedi, M.A. (2021), "Boundary conditions effect for buckling analysis of porous functionally graded nanobeam", *Adv. Nano Res.*, **10**(4), 313-325. https://doi.org/10.12989/scs.2022.44.4.503.

Bourada, M., Tounsi, A., Houari, M.S.A. and Bedia, E.A.A. (2012), "A new four-variable refined plate theory for thermal buckling analysis of functionally graded sandwich plates", *J. Sandw. Struct. Mater.*, **14**(1), 5-33. https://doi.org/10.1177/1099636211426386.

Cui, Z., Yuan, Z. and Xi, C. (2024), "Engineering the future: Exploring the dynamic behavior of nanocomposite porous beams under the influence of nanoparticles", *Struct. Eng. Mech.*, **92**(5), 513-520. https://doi.org/10.12989/sem.2024.92.5.513.

Daikh, A.A., Belarbi, M.O., Ahmed, D., Houari, M.S.A., Avcar, M., Tounsi, A. and Eltaher, M.A. (2023), "Static analysis of functionally graded plate structures resting on variable elastic foundation under various boundary conditions", *Acta Mechanica*, **234**(2), 775-806. https://doi.org/10.1007/s00707-022-03405-1.

Della Croce, L. and Venini, P. (2004), "Finite elements for functionally graded Reissner–Mindlin plates", *Comput. Method. Appl. M.*, **193**(9-11), 705-725. https://doi.org/10.1016/j.cma.2003.09.014.

Dhore, N., Khalsa, L. and Varghese, V. (2025), "Hygrothermoelastic analysis of the nano-circular plate with memory effect", *Appl. Math. Model.*, ***138***, 115797. https://doi.org/10.1016/j.apm.2024.115797.

Eltaher, M.A., Esen, I., Abdelrahman, A.A. and Abdraboh, A.M. (2024), "Dynamic response of FG carbon nanotubes nanoplates embedded in elastic media under moving point load", *Adv. Nano Res.*, **17**(3), 257-274. https://doi.org/10.12989/anr.2024.17.3.257.

Eringen, A.C. (1983), "On differential equations of nonlocal elasticity and solutions of screw dislocation and surface waves", *J. Appl. Phys.*, **54**(9), 4703-4710. https://doi.org/10.1063/1.332803.

Eringen, A.C. and Edelen, D. (1972), "On nonlocal elasticity", *Int. J. Eng. Sci.* **10**(3), 233-248. https://doi.org/10.1016/0020-7225(72)90039-0.

Esen, I. and Özmen, R. (2024), "Free and forced thermomechanical vibration and buckling responses of functionally graded magneto-electro-elastic porous nanoplates", *Mech. Based Des. Struc.*, **52**(3), 1505-1542. https://doi.org/10.1080/15397734.2022.2152045.

Fan, Y.H. and She, G.L. (2025), "Nonlinear transient response of graphene platelets reinforced metal foams beam considering initial geometrical imperfection and viscoelastic elastic foundation", *Comput. Concrete*, **35**(1), 59-70. https://doi.org/10.12989/cac.2025.35.1.059.

Farajpour, A., Yazdi, M.H., Rastgoo, A. and Mohammadi, M. (2016), "A higher-order nonlocal strain gradient plate model for buckling of orthotropic nanoplates in thermal environment", *Acta Mechanica*, **227**, 1849-1867. https://doi.org/10.1007/s00707-016-1605-6.

Hadj Mostefa, A., Merdaci, S., Bouchafa, A. and Dahamni, M. (2024), "Review of Previous Works on Functionally Graded Materials (FGM)", *South Florida J. Development, Miami*, **5**(9), 1-7. https://doi.org/10.46932/sfjdv5n9-030.

Hadji, L., Plevris, V. and Papazafeiropoulos, G. (2024), "Investigation of the static bending response of FGM sandwich plates", *J. Appl. Comput. Mech.*, **10**(1), 26-37. https://doi.org/10.22055/jacm.2023.44278.4194.

Himeur, N., Mamen, B., Benguediab, S., Bouhadra, A., Menasria, A., Bouchouicha, B., Bourada, F. and Benguediab, M. (2022), "Coupled effect of variable Winkler–Pasternak foundations on bending behavior of FG plates exposed to several types of loading", *Steel Compos. Struct.*, **44**(3), 353-369. https://doi.org/10.12989/scs.2022.44.3.353.

Karami, B., Janghorban, M. and Tounsi, A. (2019), "Galerkin's approach for buckling analysis of functionally graded anisotropic nanoplates/different boundary conditions", *Eng.with Comput.*, **35**(4), 1297-1316. https://doi.org/10.1007/s00366-018-0664-9.

Karami, B. and Karami, S. (2019), "Buckling analysis of nanoplate-type temperature-dependent heterogeneous materials", *Adv. Nano Res.*, **7**(1), 51-61. https://doi.org/10.12989/anr.2019.7.1.051.

Khorshidi, K. and Fallah, A. (2016), "Buckling analysis of functionally graded rectangular nano-plate based on nonlocal exponential shear deformation theory", *Int. J. Mech. Sci.*, **113**, 94-104. https://doi.org/10.1016/j.ijmecsci.2016.04.014.

Komarsofla, M.K., Salami, S.J., Shakeri, M. and Komarsofla, A.K. (2021), "Optimization of three-dimensional up to yield bending behavior using a full layer-wise theory for FGM rectangular plate subjected to thermo-mechanical loads", *Compos. Struct.*, **257**, 113172. https://doi.org/10.1016/j.compstruct.2020.113172.

Kumar, A.S., Kumar, S., Choudhary, P.K., Gupta, A. and Narayan, A. (2024), "Free vibration characteristics of elastic foundation-supported porous functionally graded nanoplates using Rayleigh-Ritz approach", *Int. J. Struct. Integrity*, **15**(2), 298-321. https://doi.org/10.1108/IJSI-11-2023-0114.

Liu, Z., Zhu, K., Wen, X. and Kumar, A. (2024), "Nonlinear vibration analysis of FG porous shear deformable cylindrical shells covered by CNTs-reinforced nanocomposite layers considering neutral surface exact position", *Adv. Nano Res.*, **17**(1), 61-73. https://doi.org/10.12989/anr.2024.17.1.061.

Mekerbi, M., Benyoucef, S., Mahmoudi, A., Tounsi, A., Bousahla, A.A. and Mahmoud, S. (2021), "Thermodynamic behavior of functionally graded sandwich plates resting on different elastic foundation and with various boundary conditions", *J. Sandw. Struct. Mater.*, **23**(3), 1028-1057. https://doi.org/10.1177/1099636219851281.

Meziane, M.A.A., Abdelaziz, H.H. and Tounsi, A. (2014), "An efficient and simple refined theory for buckling and free vibration of exponentially graded sandwich plates under various boundary conditions", *J. Sandw. Struct. Mater.*, **16**(3), 293-318. https://doi.org/10.1177/1099636214526852.

Najafi, M., Ahmadi, I. and Sladek, V. (2024), "A new three-dimensional model for free vibration analysis of functionally graded nanoplates resting on an elastic foundation", *Steel Compos. Struct.* **52**(3), 273-291. https://doi.org/10.12989/SCS.2024.52.3.273.

Nami, M.R., Janghorban, M. and Damadam, M. (2015), "Thermal buckling analysis of functionally graded rectangular nanoplates based on nonlocal third-order shear deformation theory", *Aerosp. Sci. Tech.*, **41**, 7-15. https://doi.org/10.1016/j.ast.2014.12.001.

Narendar, S. (2011), "Buckling analysis of micro-/nano-scale plates based on two-variable refined plate theory incorporating nonlocal scale effects", *Compos. Struct.*, **93**(12), 3093-3103. https://doi.org/10.1016/j.compstruct.2011.06.028.

Nguyen, V.L., Nguyen, V.L., Tran, M.T. and Dang, X.T. (2024), "Investigation of static buckling and bending of nanoplates made of new functionally graded materials considering surface effects on an elastic foundation", *Acta Mechanica*, 1-27. https://doi.org/10.1007/s00707-024-04127-2.

Radwan, A.F. (2019), "Effects of non-linear hygrothermal conditions on the buckling of FG sandwich plates resting on elastic foundations using a hyperbolic shear deformation theory", *J. Sandw. Struct. Mater.*, **21**(1), 289-319. https://doi.org/10.1177/1099636217693557.

Rai, S. and Gupta, A. (2024), "A novel dynamic stiffness matrix for the nonlocal vibration characteristics of porous functionally graded nanoplates on elastic foundation with small-scale effects", *J. Strain Anal. Eng. Design*, **59**(6), 408-425. https://doi.org/10.1177/03093247241252199.

Refrafi, S., Bousahla, A.A., Bouhadra, A., Menasria, A., Bourada, F., Tounsi, A., Bedia, E.A., Mahmoud, S., Benrahou, K.H. and Tounsi, A. (2020), "Effects of hygro-thermo-mechanical conditions on the buckling of FG sandwich plates resting on elastic foundations", *Comput. Concrete*, **25**(4), 311-325. https://doi.org/10.12989/cac.2020.25.4.311.

Reissner, E. and Stavsky, Y. (1961), "Bending and stretching of certain types of heterogeneous aeolotropic elastic plates", https://doi.org/10.1115/1.3641719.

Saberi, E., Amoushahi, H. and Tanzadeh, H. (2024), "Mechanical and thermal buckling of thick nanoplate with a new functionally graded porous pattern", *Arch. Civil Mech. Eng.*, **24**(2), 56. https://doi.org/10.1007/s43452-023-00856-8.

Sari, M.S., Ghaffari, S., Ceballes, S. and Abdelkefi, A. (2020), "Buckling response of functionally graded nanoplates under combined thermal and mechanical loadings", *J. Nanopart. Res.*, **22**, 1-21. https://doi.org/10.1007/s11051-020-04815-9.

Sedighi, H.M., Malikan, M., Valipour, A. and Żur, K.K. (2020), "Nonlocal vibration of carbon/boron-nitride nano-hetero-structure in thermal and magnetic fields by means of nonlinear finite element method", *J. Comput. Des. Eng.*, **7**(5), 591-602. https://doi.org/doi.org/10.1093/jcde/qwaa041.

Shen, X., Li, T., Xu, L., Kiarasi, F., Babaei, M. and Asemi, K. (2024), "Free vibration analysis of FG porous spherical cap reinforced by graphene platelet resting on Winkler foundation", *Adv. Nano Res.*, **16**(1), 11-26. https://doi.org/10.12989/anr.2024.16.1.011.

Slimani, R., Menasria, A., Ali Rachedi, M., Mourad, C., Refrafi, S., Nimer, A.A., Bouhadra, A. and Mamen, B. (2024), "A novel quasi-3D refined HSDT for static bending analysis of porous functionally graded plates", *J. Comput. Appl. Mech.*, https://doi.org/10.22059/jcamech.2024.372417.968.

Son, L.T., Vinh, P.V., Chinh, N.V. and Sedighi, H.M. (2025), "High-frequency temperature-dependent vibration of nonlocal functionally graded sandwich nanoplates resting on elastic foundations", *Mech. Adv. Mater. Struct.*, **32**(5), 957-978. https://doi.org/10.1080/15376494.2024.2358108.

Tamrabet, A., Mourad, C., Ali Alselami, N., Menasria, A., Mamen, B. and Bouhadra, A. (2024), "Efficient kinematic model for stability analysis of imperfect functionally graded sandwich plates with ceramic middle layer and varied boundary edges", *J.*

Comput. Appl. M., ***55***(2), 184-200. https://doi.org/10.22059/JCAMECH.2024.371464.947.

Tong, L., Wen, B., Xiang, Y., Lei, Z. and Lim, C. (2021), "Elastic buckling of nanoplates based on general third-order shear deformable plate theory including both size effects and surface effects", *Int. J. Mech. Mater. Design*, **17**(3), 521-543. https://doi.org/10.1007/s10999-021-09545-x.

Tounsi, A., Houari, M.S.A. and Benyoucef, S. (2013), "A refined trigonometric shear deformation theory for thermoelastic bending of functionally graded sandwich plates", *Aerosp. Sci. Tech.*, **24**(1), 209-220. https://doi.org/10.1016/j.ast.2011.11.009.

Trabelsi, S., Frikha, A., Zghal, S. and Dammak, F. (2018), "Thermal post-buckling analysis of functionally graded material structures using a modified FSDT", *Int. J. Mech. Sci.*, **144**, 74-89. https://doi.org/10.1016/j.ijmecsci.2018.05.033.

Tran, T.T. and Le, P.B. (2023), "Nonlocal dynamic response analysis of functionally graded porous L-shape nanoplates resting on elastic foundation using finite element formulation", *Eng. with Comput.*, **39**(1), 809-825. https://doi.org/10.1007/s00366-022-01679-6.

Uzun, B., Civalek, Ö. and Yaylı, M.Ö. (2023), "Vibration of FG nano-sized beams embedded in Winkler elastic foundation and with various boundary conditions", *Mech. Based Des. Struc.*, **51**(1), 481-500. https://doi.org/10.1080/15397734.2020.1846560.

Van Minh, C., Do Van, T., Van Minh, P., Nguyen, C.T., Doan, T. L. and Nguyen, H.H. (2024), "Investigation of mechanical responses of flexo-magnetic variable thickness nanoplates resting on elastic foundations, taking into account geometrical imperfections", *Front. Struct. Civil Eng.*, 1-20. https://doi.org/10.1007/s11709-024-1093-z.

Wei, C., Zhihong, T. and Linxin, P. (2024), "Linear bending analysis of functionally graded sandwich shells with the meshless method based on the layer-wise theory", **45**(5), 539-553. https://doi.org/10.21656/1000-0887.440262.

Yaghoobi, H. and Torabi, M. (2013), "Exact solution for thermal buckling of functionally graded plates resting on elastic foundations with various boundary conditions", *J. Therm. Stresses*, **36**(9), 869-894. https://doi.org/10.1080/01495739.2013.770356.

Zenkour, A.M. and Sobhy, M. (2011), "Thermal buckling of functionally graded plates resting on elastic foundations using the trigonometric theory", *J. Therm. Stresses*, **34**(11), 1119-1138. https://doi.org/10.1080/01495739.2011.606017.

CC